NASA Technical Paper 1577

Experimental Study of Acoustic Loads on an Upper-Surface-Blown STOL Airplane Configuration

Conrad M. Willis and James A. Schoenster

DECEMBER 1979

NASA

NASA Technical Paper 1577

Experimental Study of Acoustic Loads on an Upper-Surface-Blown STOL Airplane Configuration

Conrad M. Willis and James A. Schoenster
Langley Research Center
Hampton, Virginia

National Aeronautics
and Space Administration

**Scientific and Technical
Information Branch**

1979

SUMMARY

Fluctuating pressure levels have been measured on the flap and fuselage of an upper-surface-blown jet-flap airplane configuration in a wind tunnel. The model tested had turbofan engines with a bypass ratio of 3 and a thrust rating of 10 kN. Rectangular nozzles were mounted flush with the upper surface at 35 percent of the wing chord. Test parameters were flap deflection angle, jet impingement angle, angle of attack, free-stream velocity, spanwise location of the engine, and jet dynamic pressure. Load levels were high throughout the jet impingement region, with the highest levels (about 159 dB) occurring on the fuselage and near the knee of the flap. The magnitude of the forward-velocity effect appeared to depend upon the ratio of free-stream and jet velocities. Good agreement was obtained between fluctuating pressure spectra measured at jet dynamic pressures of 7 and 22 kPa when the spectra were scaled by nondimensional functions of dynamic pressure, velocity, and the empirical relationship between dynamic pressure and overall fluctuating pressure level.

INTRODUCTION

One means of obtaining powered lift for short take-off and landing (STOL) airplanes is the upper-surface-blown (USB) concept. In this approach, the jet-engine efflux becomes attached to the wing upper surface and is turned downward over a trailing-edge flap (Coanda effect), thereby increasing lift. This mode of operation produces aerodynamic and acoustic loads on the airplane that are significantly higher than those experienced by conventional airplanes (ref. 1). These higher loads indicate a need for special design efforts to prevent fatigue failures and to obtain acceptable cabin-interior noise levels. Information on the magnitude and frequency content of these fluctuating pressure loads is needed for these design efforts to be effective.

An extensive USB research program has been conducted to determine the aerodynamic performance (refs. 2 and 3), the characteristics of the fluctuating pressure loads due to jet impingement (refs. 4 to 7), and surface temperatures in the impingement region (ref. 2). The program included tests of models having rectangular nozzles (refs. 1 to 6), a D-shape nozzle (ref. 7), turbofan engines (refs. 1 to 5 and 7), and a cold air jet (ref. 6). Scaling relationships for fluctuating pressures were discussed in references 5 and 6.

Results from all these studies showed similar characteristics for the fluctuating pressure loads, but parameters for scaling relationships were not completely defined. One area in which information was lacking was the sensitivity of the load level to small changes in model geometry. The objective of the present paper is to evaluate the effects of several model-geometry parameters on the overall level and spectral content of acoustic loads measured on a USB configuration having a rectangular nozzle. Results are presented for some test conditions and measurement locations that were not included in previous papers describing these tests (refs. 1 to 7). The configuration studied was a

twin-engine, general-aviation type design having turbofan engines with rectangular nozzles mounted at about 35 percent of the wing chord.

Two models were constructed. One model, used for wind-tunnel tests, was a modified general-aviation airplane. A second model, a boiler-plate semispan model used for tests in a static test facility, was of the same scale as the wind-tunnel model but simulated only the flap and fuselage surfaces adjacent to the jet nozzle. This simpler model permitted greater versatility in examining model-geometry parameters such as jet impingement angle and engine location. In twin-engine configurations, the engines are generally mounted close to the fuselage to reduce engine-out control moments; therefore, in the present investigation, the engine-fuselage separation distance was varied on the static model to determine the effect of fuselage proximity on flap loads. Fluctuating pressure measurements were made on both flap and fuselage surfaces to determine the effects of jet impingement.

Test variables for this investigation included spanwise separation distance between the fuselage and engine, impingement angle of the jet on the flap, flap deflection angle, angle of attack, free-stream velocity, and jet dynamic pressure. Fluctuating pressures on the flap and fuselage surfaces were measured by 15 flush-mounted transducers. Results are presented in the form of overall fluctuating pressure level and power spectral density. Samples of spatial cross correlation and coherence are also presented. The relative effects of the various test parameters on the magnitude and spectral content of the fluctuating pressure loadings are analyzed, and the factors used in scaling and extrapolating test data are examined.

SYMBOLS AND ABBREVIATIONS

a	empirical constant
ΔdB	change in fluctuating pressure level
DVM	digital volt meter
FPL	fluctuating pressure level, dB
f	frequency, Hz
f_m	frequency at which amplitude of PSD reaches maximum, Hz
l	jet-exhaust run length, measured chordwise along wing surface at jet center line, cm (see fig. 3(a))
M	Mach number
n	empirical exponent for the equation $p_{rms}^2 = aq^n$
OAFPL	overall fluctuating pressure level, dB

PSD	power spectral density, $(Pa)^2/Hz$
p_{rms}	root-mean-square value of fluctuating pressure, Pa
p_r	reference fluctuating pressure, 20 μPa
q	jet dynamic pressure at nozzle exit, $\rho V_j^2/2$, Pa
q_r	reference dynamic pressure, 1 Pa
T	static temperature of jet efflux at nozzle exit, K
USB	upper surface blown
V	velocity, m/sec
w	width of jet nozzle, cm
x	distance aft of jet exit measured chordwise along wing upper surface, cm
y	distance outboard of nozzle center line, cm
y_n	nozzle location, spanwise distance from fuselage sidewall to inboard side of nozzle, cm
z	perpendicular distance from upper surface of wing, cm
α	angle of attack, deg
δ	flap deflection angle, measured between tangents to wing upper surface at jet exit and trailing edge, deg (see fig. 3(a))
θ	jet impingement angle, deg (see fig. 3(a))
ρ	density, $kg\text{-}sec^2/m^4$

Subscripts:

j	jet
max	maximum
∞	free stream

MODELS AND APPARATUS

Two models were used in this investigation. A twin-engine airplane model, complete except for empennage, was tested in the Langley full-scale tunnel to obtain aerodynamic performance data with forward-velocity effects. A second

model, a semispan model that was constructed to the same scale but simulated only the airplane surfaces washed by the jet efflux of one engine, was used for outdoor static tests. Sketches of the two models are presented in figure 1. Both models used the Pratt & Whitney JT15D-1 jet engine. This turbofan engine has a bypass ratio of about 3 and a rated thrust of 10 kN. Acoustic instrumentation consisted of flush-mounted transducers (fig. 1(a)) that measured the fluctuating component of surface pressures over the region washed by the jet efflux. The static model (fig. 1(b)) was tested in an inverted position to avoid impingment of the jet flow on the ground.

The secondary nozzle (fig. 1(b)) was rectangular in shape and had a deflector lip that aided attachment of the flow to the flap. The ratio of width to height was about 6, and nozzle area was about 0.15 m^2. The primary nozzle was elliptical in shape. The conventional inlet used for the tunnel tests was replaced by a bell-mouth inlet for the static tests. Photographs of the models are presented in figure 2. The static model (fig. 2(b)) was mounted on an exterior test stand which placed the nozzle center line 1.7 m above the ground. A view of the static model in one of the fuselage configurations is shown in figure 2(c). Additional details concerning the models are given in references 2 and 3.

Configurations

A list of the test configurations and sketches defining model geometry and the nomenclature used in this paper are presented in figure 3. The model-geometry parameters of flap deflection angle δ, jet impingement angle θ, run length of the jet efflux l, and the spanwise clearance between the nozzle and fuselage y_n, were changed to obtain the 10 test configurations listed in the table in figure 3(a). Most of the configuration changes were made on the static-test-stand model because of the simpler construction. The flap of the static-test-stand model was not swept or tapered but had the same nominal geometry as that for the wind-tunnel-model flap at the engine center-line span station. However, the procedures used in fabrication and assembly of the flap resulted in minor differences in length and curvature, as indicated in the bottom sketch of figure 3(b). A curved plate, representing a section of the fuselage sidewall, was bolted to the flap for part of the tests. Relative spanwise locations of the engine on the wing were simulated by repositioning the fuselage section. The flap could be rotated about a hinge line lying along the lower edge of the nozzle exit to change impingement angle θ (fig. 3(a)). Impingement angle for this test was defined as the angle between a chordwise tangent to the flap upper surface at the nozzle exit plane and the direction of the thrust force vector measured with the jet exhausting into free space before installation of the flap (fig. 3(a)). Run length was changed by removing the trailing-edge section of the flap. A rectangular nozzle, 94.0 cm wide by 15.7 cm high, was used for all configurations.

Instrumentation

Fluctuating pressure transducers were mounted flush with the airplane surfaces at the locations indicated in figure 4. The flap locations are specified

in terms of x and y dimensions, which indicate the respective distances, measured along the airplane surface, that the transducer is aft of the nozzle exit and outboard of the nozzle center line. Locations for the fuselage transducers (fig. 4(c)) are given in terms of both x and the perpendicular distance from the trace of the flap intersection with the fuselage sidewall. Transducer installation details are presented in figure 5. The transducer used is temperature compensated for the 270 to 500 K range and is capable of withstanding operation at slightly higher temperatures. The sensing element is a strain-gaged diaphragm having a natural frequency of about 100 kHz. The transducer was bonded into a threaded fitting, with the protective grid covering the diaphragm flush with the end of the fitting. The reference side of the diaphragm was connected to a point on the airfoil surface through a length of small-diameter tubing to remove static pressure from the measurement.

A schematic drawing of the instrumentation setup is presented in figure 6. A high-pass filter was used to remove the low-frequency portion of the signal up to 20 Hz. The data were recorded on two 14-channel FM tape recorders with recording speeds of 152 cm/sec. A narrow-band spectrum analyzer was used to make a preliminary check of the data as they were being recorded. Other quantities measured in addition to fluctuating pressure were thrust, static pressure and temperature over the flap, and the dynamic pressure and temperature of the jet exhaust.

TESTS

Ten model configurations were tested. (See fig. 3(a).) Test conditions are listed in table I. Each configuration was operated at four or five thrust levels to obtain dynamic pressures at the jet exit that ranged from about 3 kPa at engine-idle condition to about 22 kPa at the highest speed permitted by the temperature limit for the engine bearings. The transducers were calibrated with an acoustic calibrator after installation on the model and again at the end of the investigation. As an additional check on the system calibration, a known voltage was applied at a point between the transducers and amplifier at the start of testing each day. The procedure followed in recording the data was to adjust engine fuel-flow rate to obtain the desired jet dynamic pressure, monitor signal level from the fluctuating pressure transducers and adjust amplifier gain setting to obtain the proper recording level, wait a few seconds for flap surface temperature to stabilize, and then record about 30 sec of data. Aerodynamic performance data reported in previous papers (ref. 2 and 3) were also acquired for each test condition.

ACCURACY

Acceptance specifications for the fluctuating pressure transducers were (1) repeatability of within ±0.25 percent of full-scale output, (2) a natural frequency above 100 kHz, (3) thermal zero shifts of less than 20 percent of full scale over an operating range of 270 to 530 K, and (4) an acceleration sensitivity of less than 0.008 percent of full scale/gravitational unit.

Because of the severe temperature and vibration environment and the complex transducer-mounting requirements, it was difficult to obtain an accurate absolute calibration of the transducers. However, random scatter of the data was small and the repeatability was good. Fluctuating pressure data plotted with p_{rms} as a function of log q had average deviations of less than 0.1 dB (re: 20 log (p/p_r)) from the best fitting straight line, and data from repeated tests agreed with ±0.3 dB. Therefore it is believed that the changes in OAFPL due to model configuration changes can be measured to an accuracy of about ±0.5 dB.

RESULTS AND DISCUSSION

The fluctuating pressure data were processed to obtain overall levels and power spectra, and a few test conditions and measurement locations were selected for further data reduction to obtain cross-correlation and coherence functions. The data were then analyzed and compared to determine the effects of the various test parameters. A tabulation of the model configuration code number and test conditions for each test run is presented in table I, and the corresponding OAFPL measurements are presented in tables II and III.

The order of presentation of the results begins with flap data, followed by fuselage data. Overall level effects of all the test parameters are discussed before considering the spectra and cross correlation. The flap test environment, consisting of static pressure and temperature on the flap surface and jet efflux temperature and velocity at the nozzle exit, is presented in figures 7 to 9. Flap OAFPL is presented in figures 10 to 17. Fluctuating pressure spectra for flap locations under various conditions are presented in figures 18 to 22. Figure 23 illustrates the collapse of normalized spectra. Correlation-coefficient and coherence functions are presented in figures 24 and 25. Fuselage data are presented in figures 26 to 29.

Flap Environment

Data defining the flap environment from the nozzle exit to the trailing edge are presented in figures 7, 8, and 9. Jet dynamic pressure for the test ranged from about 3 kPa to 22 kPa (fig. 7), with velocity, temperature, and Mach number ranges of about 100 to 300 m/sec, 500 to 700 K, and 0.2 to 0.6, respectively. The measured quantities were temperature and dynamic pressure, from which velocity and Mach number were then calculated, with the ambient pressure assumed to be that for standard sea-level conditions. Jet temperatures for the wind-tunnel test were about 30 to 70 K higher than for the static test. This higher temperature was due in part to a higher inlet temperature produced by recirculation of the air within the wind tunnel. Another possible source of temperature differences is a change in the relative alinement of primary and secondary nozzles during reassembly after transfer between models. A slight difference occurring in nozzle alinement could affect the bypass ratio and the completeness of mixing and thus contribute to the temperature difference. The higher temperature of the wind-tunnel model produced jet velocities that

were about 6 percent higher than those for the static model at a given jet dynamic pressure.

Surface temperatures on the flap are presented in figure 8. Temperatures over the impinged region varied irregularly by as much as 175 K, indicating the incomplete mixing of the primary, bypass, and entrained gas flows. Surface temperatures were somewhat higher for the wind-tunnel model, as would be expected from the higher exit temperatures. All temperatures measured were at least 150 K below the exit temperature; however, the 522 K maximum temperature measured on the wing probably prohibits the use of aluminum alloy structural materials within the impinged area (ref. 8).

Figure 9 presents the static-pressure distribution over the flap upper surface for $q = 22$ kPa and $V_\infty = 0$. Arrows drawn from the location of each measurement point indicate the direction and magnitude of the static-pressure loading on the flap at the given location. There is a small area of positive pressure, or negative lift, located on the nozzle center line near the exit that probably represents an impingement point for some incompletely mixed flow from the primary nozzle. Negative gage pressures over the aft two-thirds of the flap surface indicate attachment and turning of the jet sheet by the flap.

Overall Level of Flap Fluctuating Pressure Loads

Distribution over flap.- Load distributions along the flap center line over the range of jet dynamic pressure with no forward speed are presented in figure 10. Loads are high enough to be significant to the structural design (ref. 1) over the entire flap length, with the highest loading occurring at the flap knee. Figure 11 compares measurements of fluctuating pressure along the nozzle center lines of the wind-tunnel and static models to show that minor differences in flap shape (fig. 3(b)) did not produce substantial differences in flap loads. The pressures are presented in the nondimensional form p_{rms}/q to reduce the range of ordinate scale and also to partially compensate for small differences in the values of q at which measurements for the two models were made. The data from the two configurations appear to agree fairly well for both levels of jet dynamic pressure. The differences in level for $q = 11$ kPa and $q = 22$ kPa are small near the trailing edge where mixing is probably most complete. Near the knee of the flap, the differences are larger, which indicate that the average jet dynamic pressure q is not directly proportional to fluctuating pressure p_{rms} at all measurement locations.

Effect of jet dynamic pressure.- Figure 12(a) presents a comparison of OAFPL at the 11 flap measurement locations for a jet dynamic-pressure range of 3.3 kPa to 22.3 kPa. The OAFPL is directly proportional to some power of dynamic pressure q at all measurement locations. The highest load levels were measured at locations near the knee of the flap, as noted in the discussion of the previous figures. Variation of load level with spanwise measurement location was much smaller than the chordwise variation. There appear to be some small differences between the slopes of the faired lines for the various locations. These differences are shown in greater detail in figure 12(b), which repeats the data for three locations in a slightly different format. A

common intersection point for the four least-squares fitted lines was obtained by setting the zero ΔdB reference level for each measurement location equal to the dB level of the fitted line at $q = 3$ kPa. For the purposes of scaling and extrapolating data, OAFPL is sometimes considered to vary linearly with the square of jet dynamic pressure (ref. 1); therefore, this relationship, expressed in the form of $p^2 = aq^2$, is shown in figure 12(b) for comparison with the measured data. Slopes of the lines, or values of the exponent n, for $p^2 = aq^n$ are indicated in the key of the figure. The values of n ranged from 1.7 to 2.0 for flap locations, and from 1.8 to 2.1 for fuselage locations. This deviation of the calculated slope from the nominal value of two may indicate a nonlinear relationship between the value of q at the exit, which is used for the plotting parameter, and the local value of q as the flow accelerates over the curved surface at location 6.

Effect of impingement angle.- The effect of a 6° change in impingement angle on OAFPL is shown in figure 13. The average effect for all measurement locations over the range of jet dynamic pressure was near zero. Changes in level of about $\pm 1\text{-}1/2$ dB occurred at a few measurement locations because changing the impingement angle moved a different streamline over the transducer in the imperfectly mixed flow from the nozzle. In real airplane design, the impingement angle selected would probably be the minimum angle required for attachment of flow for the deflected flap condition. For this reason, most of the testing was conducted with an impingement angle of 5°; however, the present configuration appears to experience little penalty in OAFPL from using an impingement angle larger than that required for flow attachment.

Effect of airspeed.- The effect of airspeed on flap loads is shown in figure 14(a) by comparing the loads over the jet dynamic-pressure range at a free-stream velocity of 16 m/sec with those for the static condition. There were small decreases in loads with airspeed at most measurement locations; at a jet dynamic pressure of 22 kPa, the average reduction from the load at zero airspeed was 0.5 dB. The increased load occurring at measurement location 5 could be due to airspeed effects on the jet boundary that may have moved the jet free-stream interface closer to the transducer. The effect of airspeed on OAFPL varied with jet dynamic pressure, and this effect is presented in figure 14(b). For the limited range of data available, the amount of load reduction from the static condition (ΔdB) appears to vary fairly smoothly as a function of the ratio of free-stream to jet velocity V_{∞}/V_j.

Effect of angle of attack.- Overall fluctuating pressure levels at three locations for an airspeed of 15 m/sec and the range of angle of attack investigated are presented in figure 15(a). All the measurement locations showed little or no change in fluctuating pressure for angles of attack in the range of $\pm 10^{\circ}$. At higher angles of attack, a few locations showed a slight change in fluctuating pressure level; for example, the OAFPL at location 5 decreased while the level for location 1 increased. However, the change at both locations moved the level closer to the OAFPL measured at $V_{\infty} = 0$. This decrease in airspeed effect at high angles of attack is illustrated more clearly in figure 15(b) by presenting the ratio of the magnitude of the airspeed effect at a given α to the magnitude at $\alpha = 0^{\circ}$. This figure shows that high angles of attack decrease the absolute value of the airspeed effect for both location 1, where airspeed decreased the OAFPL, and location 5, where airspeed increased OAFPL.

Effect of flap deflection.- Overall fluctuating pressure levels for the 32° and 74° flaps are compared in figure 16. Chordwise distribution of the flap load at the nozzle center-line station for a jet dynamic pressure of about 22 kPa is presented in figure 16(a). Relative flap profile and transducer locations for the data presented are indicated at the top of the figure. Loads on the aft, movable portion of the flap increased with flap deflection, although loading at the two forward transducers on the fixed part of the flap did not change. Figure 16(b) presents a comparison of loads for the two flap deflections over the range of jet dynamic pressure. Loads for the 74° flap deflection were up to 1.7 dB higher (transducer location 5) than those for 32° deflection, and the change in load with flap deflection for a given location was nearly independent of dynamic pressure.

Effect of fuselage.- The static model was tested with the engine located at three different spanwise locations to determine whether flap loads were affected by the nearness of the jet nozzle to the fuselage. Figure 17 compares flap OAFPL data for the inboard edge of the nozzle located at points 1 cm, 30 cm, and 60 cm outboard of the fuselage sidewall with data obtained with the fuselage removed from the model. Flap loads for the 1-cm separation distance (fig. 17(a)) were about 0.5 dB less than those for the fuselage-off condition over most of the flap for a jet dynamic pressure of 22 kPa. The effect of the fuselage over the test range of jet dynamic pressure is presented in figures 17(b) and 17(c). The reduction of flap loads due to the presence of the fuselage remained at about the previously noted (fig. 17(a)) 0.5-dB level at most locations throughout the test range of jet dynamic pressure (fig. 17(b)), and was also unaffected by changing the nozzle-fuselage separation distance from 1 cm to 30 cm. Larger reductions, about 2.5 dB, were measured by the transducer closest (8 cm) to the fuselage (fig. 17(c)). This larger reduction is assumed to be due to a thicker jet boundary layer at the fuselage-wing intersection which shielded this area from jet impingement. When the fuselage was moved to obtain the next test location (corresponding to a distance of 38 cm from fuselage to transducer), the data from location 7 showed the same 0.5-dB reduction as all the other locations. Thus, the data presented in figure 17 indicate that the fuselage effects on flap loads are small for a rectangular nozzle, and valid flap acoustic-loads data for most of the flap area can be obtained with a simplified model without a fuselage.

Spectral Distribution of Loads

Variation of PSD with location.- Fluctuating pressure power spectral density (PSD) at a jet dynamic pressure of 22 kPa is presented in figure 18 for several measurement locations on the static model. Transducer locations are indicated in the sketch on the left side of the figure. The overall level of each location is identified by the numbers on the right side of the spectrum. Spectra from locations nearest the nozzle are presented in figure 18(a). Locations near the nozzle (locations 1 to 4) had high spectrum levels over a wider frequency range than other locations. There also appeared to be a trend toward dual peaks in the spectra. Spectra from locations on the engine center line (locations 3, 6, 8, 10, and 11) are presented in figure 18(b). The double peak has disappeared at location 6, and the frequency of the PSD maximum amplitude decreases with distance downstream from the nozzle exit. Spectra for three

locations (7, 8, and 9) near the flap knee are presented in figure 18(c). Locations near the knee had the highest overall levels and the sharpest spectral peaks. The frequency of the maximum spectral level does not appear to vary with spanwise location.

Variation of PSD with jet dynamic pressure.- Fluctuating pressure spectra for the five test values of jet dynamic pressure are compared in figure 19. The table at the top of the figure lists some statistics for the spectra. Both the magnitude and frequency for PSD maximum amplitude increase with jet dynamic pressure. Over the test range of jet dynamic pressure, both the jet velocity and the frequency of the spectrum peak increased by a factor of about 3, but the general shape of the spectra on a logarithmic frequency scale showed little change at a given location on the flap. On the high side of the PSD peak, the spectra decayed at about 5 or 6 dB/octave.

Effect of jet impingement angle.- Spectra for the two test values of jet impingement are compared in figure 20. Changing the impingement angle from 5° to 11° had little effect on the PSD, as might be expected from the lack of change in OAFPL previously discussed (fig. 13). Most of the minor change that did occur was on the low-frequency side of the PSD maximum. The frequency of the maximum was not changed.

Effect of airspeed.- Spectra for airspeeds of 0 m/sec and 15 m/sec are compared in figure 21. Airspeed reduced the level of the spectrum on the low-frequency side of the peak and had the most effect at the lowest values of jet dynamic pressure, which is in agreement with the trend noted for overall levels in figure 14. Airspeeds of about 15 m/sec had no effect on the high-frequency part of the spectrum, and the frequency of the peak was unchanged except for locations near jet free-stream interface (location 5, fig. 21(a)).

Effect of flap deflection.- Figure 22 presents a comparison of spectra for flap deflections of 32° and 74°. The set of spectra in the top half of the figure was measured at location 4 on the fixed part of the flap (see figs. 3 and 4), and the set in the lower half was measured on the movable portion of the flap. Spectra from measurement locations on the fixed part of the flap were unaffected by the change in flap deflection. Spectra for locations on the movable part of the flap increased in level with increased flap deflection over the entire frequency range, but the greatest amount of change occurred at the low-frequency end of the spectrum.

Normalizing and Scaling

Spectral data are commonly presented in some normalized form to facilitate comparisons with other tests and to aid the designer in extrapolating model test results to operating conditions. Many researchers have made analytical and empirical attempts to determine the flow parameters that are best suited for the scaling of fluctuating pressure data (e.g., refs. 4, 6, and 9).

Reference 10 shows that for dynamically similar systems having the same velocity, temperature, and density, the OAFPL is the same for any model size and that the power spectra is also independent of model size if presented in

the form of one-third octave or other constant percentage bandwidth levels plotted as a function of the product of frequency and a characteristic length w of the model. Increasing the jet velocity increases the overall level of the fluctuating pressures, and the frequency of the spectra peak increases approximately proportional to the velocity. Therefore, a velocity term is usually added to provide a nondimensional frequency parameter fw/V_j known as Strouhal number. If the spectra are presented as PSD rather than in constant percentage bandwidths, the levels must be scaled by the inverse of the w/V_j factor used on the frequency scale to remove the effect of model size and velocity. The PSD is generally made nondimensional by dividing by q^2 to obtain the expression $PSD(V_j/wq^2)$. The dynamic pressure used is frequently measured at the jet exit because this is the most convenient point. However, this introduces some uncertainty into the scaled spectrum levels because the local value of q at the measurement location is dependent on model geometry.

In the present paper, spectra being compared are presented on an ordinate scale having normalized units of $PSD(V_j/wq^2)(q_r/q)^{n-2}$. The characteristic length w used was the nozzle width, and n is the empirical constant calculated for each measurement location by curve fitting $p^2 = aq^n$ to the experimental data. (See fig. 12(b).) This procedure establishes the correct relative levels for the spectra for all locations based on the measurement of dynamic pressure at a single location.

Figure 23 presents a comparison of normalized spectra for $q = 6.7$ kPa and 22.3 kPa at eight measurement locations. The collapse of the nondimensional data is considered to be good at all measurement locations, with little difference in either the level or frequency of the peak for the two conditions. However, the collapse of the data was slightly better for frequencies above the spectra peaks.

Fluctuating Pressure Cross Functions

Cross-correlation coefficients.- Cross correlation between fluctuating pressure data from various pairs of measurement locations is presented in figure 24. Cross correlation was generally too low to be of much significance; the maximum value observed was a correlation coefficient of about 0.4 at a time delay of 1.6 msec (fig. 24(a)) for measurement locations 8 and 6. Figure 24(b) presents the correlation coefficients for 10 pairs of measurement locations on the static model. The arrows show the pressure disturbance propagation direction indicated by the sign of the time delay at the maximum value of the cross-correlation coefficient for fluctuating pressures at the two locations. The number adjacent to the arrow is the maximum value of the correlation coefficient for data from the given pair of measurement locations at a dynamic pressure of $q = 22$ kPa. Correlation was lowest for data from locations separated by the flap knee. Figure 24(c) presents data from the wind-tunnel model for $V_\infty = 0$ and 16 m/sec to show that forward velocity had little effect on cross-correlation coefficients in the jet impingement region.

Coherence.- The coherence function for fluctuating pressure data from three pairs of measurement locations on the static model is presented in figure 25. Coherence was high enough to be significant only over narrow frequency ranges

that usually matched the PSD peak frequencies. The PSD for each location is shown for reference at the top of the figure.

Fuselage Loads

Fluctuating pressure loads on the fuselage were measured at the four locations indicated in figure 26. Location 12 is within the impingement region for both the 32° and 74° flap deflections. The amount of impingement on locations 13 and 14 is affected by flap deflection, and location 11 is under the wing and completely removed from the impingement region. A comparison of OAFPL at the four locations over the test range of dynamic pressure is presented in figure 27(a). Location 12, 30 cm above the flap, experienced loads up to 159 dB, about equal to the highest loads measured on the flap. Loads below the wings at location 11 were not significant. The effects of airspeed and flap deflection on OAFPL are presented in figure 27(b). Airspeed had little effect on fuselage OAFPL. Decreasing the flap deflection from 74° to 32° directed more of the jet efflux toward location 13 and increased OAFPL by about 2 dB. Normalized PSD for the fuselage fluctuating pressure loads is presented in figure 28. Spectra for the three locations in the impingement region exhibited good collapse when normalized by jet exit velocity and dynamic pressure. Spectra for the under-the-wing location did not collapse. Spectra shapes for the two conditions are very similar and OAFPL varied smoothly with q (fig. 27(a)), but the frequency of spectrum peak remained constant over the test range of jet dynamic pressure. This frequency is assumed to be one of the natural frequencies of the structure.

The effect of airspeed on fluctuating pressure PSD is presented in figure 29. The effect is about the same as previously noted for flap locations. Airspeed reduces the low-frequency level; at frequencies above the spectrum peak, airspeed has little effect.

CONCLUSIONS

A wind-tunnel and static-test-stand investigation of the acoustic loads occurring on a rectangular nozzle, upper-surface-blown configuration has been conducted. The models had JT15D-1 engines which were operated over a nozzle-exit jet dynamic-pressure range of about 3 kPa to 22 kPa to evaluate the effect on fluctuating pressure load levels of changes in various model-geometry parameters. Analysis of the amplitude and frequency content of fluctuating pressure loads measured in the impingement region of the jet exhaust has led to the following conclusions:

1. Fluctuating pressure loads on the airplane surfaces are high throughout the region washed by the jet efflux, up to 159 dB for a jet-exit dynamic pressure of 22 kPa.

2. Fuselage sidewall areas lying within the impingement region experienced loadings equal to the highest loading measured directly behind the engine on the flap.

3. Good agreement was obtained between fluctuating pressure spectra measured at jet dynamic pressures of 7 kPa and 22 kPa when the spectra were scaled by nondimensional functions of dynamic pressure, length, velocity, and an empirical relationship between dynamic pressure and the overall fluctuating pressure level.

4. Both angle-of-attack and forward-velocity effects were small for the airspeed range of 0 m/sec to 16 m/sec covered in this test. The magnitude of the effect appeared to be a function of the ratio of free-stream to jet velocity.

5. Small increases in load occurred with increasing jet impingement angles and increasing flap deflection angles.

6. Highest flap loads occurred near the knee of the flap for all test conditions.

Langley Research Center
National Aeronautics and Space Administration
Hampton, VA 23665
October 19, 1979

REFERENCES

1. Mixson, John S.; Schoenster, James A.; and Willis, Conrad M.: Fluctuating Pressures on Aircraft Wing and Flap Surfaces Associated With Powered-Lift Systems. AIAA Paper 75-472, Mar. 1975.

2. Staff of Langley Research Center: Wind-Tunnel Investigation of Aerodynamic Performance, Steady and Vibratory Loads, Surface Temperatures, and Acoustic Characteristics of a Large-Scale Twin-Engine Upper-Surface Blown Jet-Flap Configuration. NASA TN D-8235, 1976.

3. Shivers, James P.; and Smith, Charles C., Jr.: Static Tests of a Simulated Upper Surface Blown Jet-Flap Configuration Utilizing a Full-Size Turbofan Engine. NASA TN D-7816, 1975.

4. Schoenster, James A.; Willis, Conrad M.; Schroeder, James C.; and Mixson, John S.: Acoustic-Loads Research for Powered-Lift Configurations. Powered-Lift Aerodynamics and Acoustics, NASA SP-406, 1976, pp. 429-443.

5. Willis, Conrad M.; Schoenster, James A.; and Mixson, John S.: Acoustics Loads on Upper-Surface-Blown Powered-Lift Systems. J. Aircr., vol. 15, no. 10, Oct. 1978, pp. 670-675.

6. Haviland, J. K.; and Herling, W. W.: Modeling Techniques for Jet Impingement. AIAA Paper 77-591, June 1977.

7. Pappa, Richard S.: Surface Fluctuating Pressure Measurements on 1/4-Scale YC-14 Boilerplate Model. AIAA Paper 77-592, June 1977.

8. Alcoa Aluminum and Its Alloys: Aluminum Co. of America, 1950.

9. Franken, Peter A.; Kerwin, Edward M., Jr.; and the Staff of Bolt Beranek and Newman, Inc.: Methods of Flight Vehicle Noise Prediction. WADC Tech. Rep 58-343, DDC Doc. No. AD 205 776, U.S. Air Force, Nov. 1958.

10. Bies, David A.; and Franken, Peter A.: Notes on Scaling Jet and Rocket Noise. J. Acoust. Soc. America, vol. 33, no. 9, Sept. 1961, pp. 1171-1173.

TABLE I.- TEST CONDITIONS

Wind-tunnel model						Static-test model			
Model configuration (a)	Run	V_∞, m/sec	α, deg	q, kPa	M	Model configuration (a)	Run	q, kPa	M
1.1	2694	0	0	5.5	0.28	2.1	1022	3.3	0.214
	2693			11.7	.40		1026	6.5	.301
	2692			17.2	.49		1025	11.7	.405
	2691			22.8	.56		1024	16.0	.473
	2759	18	-5	22.8	.56		1023	22.2	.557
	2703	17	0	11.7	.40				
	2783	18		11.7	.40	2.2	1047	3.2	0.214
	2700			17.2	.49		1051	6.3	.297
	2695			22.8	.56		1050	11.5	.402
	2760						1049	15.8	.471
	2773						1048	22.8	.565
	2704	17	10	11.0	.39				
	2779	18		11.7	.40	2.3	1037	3.3	0.215
	2701	17		17.2	.49		1041	7.0	.312
	2698	18		22.8	.56		1040	12.1	.412
	2776	18		22.1	.56		1039	16.5	.481
	2705	15	25	11.0	.39		1038	23.3	.572
	2702	16		17.2	.49				
	2699	16		22.8	.56	2.4	1042	3.4	0.219
							1046	6.6	.303
1.2	2052	0	0	4.8	0.26		1045	11.9	.408
	2049			11.0	.39		1044	16.1	.475
	2046			16.5	.48		1043	24.0	.580
	2043			22.1	.56				
	2036	16	-5	16.5	.48	2.5	1017	3.3	0.214
	1629	16	-5	22.8	.56		1021	6.7	.306
	1552	15	0	5.5	.28		1020	11.9	.409
	1561			11.0	.39		1019	16.2	.477
	1570			11.7	.40		1018	22.3	.559
	2037	16		16.5	.48				
	2030	16		22.1	.56	2.6	1027	3.3	0.214
	1301	15		22.8			1031	6.6	.304
	1631	16		22.8			1030	11.8	.406
	1632	15	5	22.1			1029	16.0	.474
	1555	14	10	5.5	.28		1028	21.8	.553
	1564	14		11.0	.39				
	1573	15		11.0	.39	2.7	1032	3.2	0.212
	1304			22.8	.56		1036	6.4	.300
	1633						1035	11.7	.405
	1634		15				1034	15.9	.472
	1558	14	20	4.8	.26		1033	21.8	.549
	1567			11.0	.39				
	1576			11.0	.39	2.8	1012	3.2	0.214
	1635	15		22.8	.56		1016	6.7	.306
	2042		25	16.5	.48		1015	11.9	.409
	1636			22.8	.56		1014	16.2	.476
	2035			22.1	.56		1013	22.3	.558

[a]Model geometry corresponding to the configuration number is tabulated in figure 3(a).

TABLE II.- OVERALL FLUCTUATING PRESSURE LEVEL

FOR WIND-TUNNEL MODEL

Run	Overall fluctuating pressure level, dB, for wind-tunnel model at measurement locations -								
	1	2	3	4	5	6	7	8	9
2694	138.9	139.3	146.0	143.5	144.1	143.2	-----	-----	-----
2693	144.9	144.9	151.9	149.5	150.1	149.0	-----	-----	-----
2692	147.9	147.5	154.8	152.1	153.2	151.8	-----	-----	-----
2691	149.9	149.7	157.1	154.1	155.4	154.1	-----	-----	-----
2759	149.1	149.0	156.5	153.5	154.4	153.3	-----	-----	-----
2703	143.8	143.9	150.8	148.3	148.1	148.1	-----	-----	-----
2783	143.6	143.5	150.6	148.0	147.9	147.9	-----	-----	-----
2700	147.1	147.1	154.4	151.5	152.0	151.4	-----	-----	-----
2695	149.5	149.3	157.0	153.8	154.6	153.5	-----	-----	-----
2760	149.0	149.0	156.3	153.6	154.2	153.4	-----	-----	-----
2773	149.0	148.9	156.3	153.4	154.4	153.4	-----	-----	-----
2704	143.8	144.1	149.8	148.7	147.9	148.2	-----	-----	-----
2779	143.7	143.9	149.7	148.4	148.1	148.2	-----	-----	-----
2701	146.9	146.9	153.5	151.6	151.6	151.3	-----	-----	-----
2698	149.0	149.1	156.0	153.5	154.3	153.6	-----	-----	-----
2776	148.8	148.6	155.7	153.3	154.2	153.4	-----	-----	-----
2705	143.9	143.9	148.8	148.5	147.8	148.5	-----	-----	-----
2702	147.5	147.2	153.0	151.9	152.2	151.6	-----	-----	-----
2699	149.6	149.0	155.5	153.6	154.4	153.8	-----	-----	-----
2052	139.0	139.2	145.7	143.7	144.0	144.7	144.2	141.2	137.6
2049	144.7	144.6	151.5	149.1	150.2	150.7	149.7	146.9	143.3
2046	147.8	147.6	154.9	152.1	153.9	153.7	152.6	150.4	146.7
2043	149.7	149.4	156.9	153.9	156.3	155.7	154.6	152.7	148.9
2036	147.1	146.7	154.1	151.3	155.4	153.1	151.9	150.0	146.1
1629	149.3	149.1	156.5	153.5	157.9	155.2	153.9	152.2	-----
1552	137.3	137.8	143.3	142.4	144.8	143.0	141.7	139.4	-----
1561	143.8	-----	150.8	148.4	151.8	149.3	148.7	146.2	-----
1570	143.9	144.1	151.0	148.6	152.2	149.8	148.8	146.5	-----
2037	146.9	146.8	154.0	151.5	155.4	153.0	151.7	149.6	145.9
2030	-----	149.2	156.3	153.6	157.9	155.2	154.0	152.2	148.4
1301	149.4	149.2	156.6	153.6	157.6	155.5	154.1	152.6	-----
1631	149.2	149.0	156.5	153.4	158.1	155.2	153.9	152.4	-----
1632	149.2	149.0	156.3	153.5	158.1	155.5	154.1	152.5	-----
1555	137.1	137.7	141.5	142.5	144.4	143.1	142.0	139.3	-----
1564	144.0	143.9	149.6	148.4	151.7	149.8	148.4	146.2	-----
1573	144.0	144.0	149.7	148.5	152.2	149.7	148.6	146.3	-----
1304	149.6	149.2	156.2	153.5	157.6	155.6	154.3	152.9	-----
1633	149.3	149.1	155.9	153.6	158.2	155.5	153.9	152.3	-----
1634	149.4	149.1	155.6	153.6	157.9	155.5	154.1	152.4	-----
1558	137.3	137.5	141.3	142.2	144.2	143.0	141.7	139.5	-----
1567	144.3	144.1	149.9	148.6	151.7	150.1	148.8	146.5	-----
1576	144.0	144.0	149.3	148.5	152.1	150.0	148.8	146.5	-----
1635	149.8	149.1	155.8	153.5	157.8	155.4	154.0	152.5	-----
2042	147.8	147.0	153.9	151.8	155.2	153.4	152.1	150.1	146.6
1636	150.0	149.2	156.6	153.7	156.8	155.7	154.1	152.8	-----
2035	150.0	149.3	156.3	153.8	157.1	155.8	154.1	152.6	149.1

TABLE III.- OVERALL FLUCTUATING PRESSURE LEVEL

FOR STATIC-TEST MODEL

Run	Overall fluctuating pressure level, dB, for static-test model at measurement locations -										
	1	2	3	4	5	6	7	8	9	10	11
1022	134.1	135.2	135.8	133.8	141.4	139.8	142.5	141.4	143.3	139.7	-----
1026	139.1	140.0	140.3	138.8	146.1	144.1	147.3	145.9	147.8	144.6	-----
1025	143.9	145.1	145.1	143.9	150.8	148.6	151.7	150.0	152.5	149.7	-----
1024	146.9	147.7	147.5	146.5	153.2	150.5	154.2	152.4	154.8	151.9	-----
1023	151.9	151.0	150.6	149.9	156.2	153.4	157.0	155.4	157.8	155.5	-----
1047	133.1	134.7	135.2	133.4	-----	139.0	-----	140.6	142.8	140.0	-----
1051	138.5	139.9	140.3	138.7	-----	143.9	-----	145.6	148.2	145.3	-----
1050	143.6	144.9	145.1	144.1	-----	148.6	-----	150.0	152.7	150.1	-----
1049	146.8	147.6	147.5	146.5	-----	150.5	-----	152.4	155.0	153.0	-----
1048	151.9	150.6	150.3	149.7	-----	153.1	-----	154.9	157.6	155.2	-----
1037	133.0	134.3	135.2	133.0	140.0	139.5	139.6	141.2	142.9	139.5	-----
1041	138.7	140.3	140.7	139.1	146.1	144.3	145.5	146.0	148.2	145.6	-----
1040	143.5	145.1	145.3	144.2	151.0	148.3	149.9	150.3	153.2	150.0	-----
1039	146.5	147.9	147.7	146.7	153.1	150.7	152.6	152.6	155.4	152.7	-----
1038	151.2	150.9	150.4	149.6	155.6	153.3	155.2	155.2	157.8	155.1	-----
1042	133.0	134.5	135.1	133.3	141.4	138.8	142.0	140.7	143.0	139.7	-----
1046	138.5	140.1	140.4	138.9	146.3	143.9	147.1	145.8	147.9	145.2	-----
1045	143.4	145.2	145.3	144.2	151.2	148.6	151.9	150.5	152.4	150.0	-----
1044	146.2	147.6	147.5	146.7	153.4	150.6	154.1	152.3	154.7	152.1	-----
1043	151.3	151.2	150.6	149.8	156.4	153.3	157.0	155.1	157.6	155.5	-----
1017	134.8	135.4	135.9	133.8	141.8	139.5	142.2	140.9	142.9	139.7	135.1
1021	140.3	141.2	141.4	139.9	147.2	144.9	148.1	146.6	148.8	146.2	141.4
1020	145.3	146.2	145.9	145.2	152.3	149.3	152.8	151.0	153.4	150.8	146.0
1019	148.4	148.7	148.3	147.5	154.3	151.5	155.1	153.1	155.5	153.3	148.6
1018	152.3	151.3	151.0	150.2	156.4	153.6	157.7	155.5	157.8	155.8	150.8
1027	135.2	135.8	136.1	135.7	142.4	140.5	142.1	141.4	143.4	139.7	-----
1031	140.8	141.2	141.4	141.5	148.1	145.7	148.0	146.2	149.3	144.8	-----
1030	145.6	146.0	145.8	146.2	152.6	150.0	152.3	151.1	153.5	150.1	-----
1029	148.9	148.4	148.1	148.7	154.9	152.2	154.5	153.6	156.0	152.8	-----
1028	152.7	150.5	150.1	151.0	157.2	154.2	157.1	155.6	158.1	154.7	-----
1032	134.6	135.7	135.6	135.6	-----	140.2	-----	141.3	143.0	139.7	-----
1036	140.0	140.6	141.1	141.1	-----	145.8	-----	146.5	148.9	145.2	-----
1035	145.4	146.0	145.8	146.3	-----	150.0	-----	151.1	153.5	150.4	-----
1034	148.9	148.3	148.0	148.6	-----	152.4	-----	153.6	155.8	153.2	-----
1033	152.8	150.7	150.2	150.9	-----	154.2	-----	155.6	158.0	155.4	-----
1012	134.9	136.0	136.2	135.2	141.8	139.8	141.4	140.9	141.7	139.4	134.0
1016	140.6	141.4	142.2	141.7	148.2	145.9	147.7	146.7	147.9	145.5	140.6
1015	145.8	145.9	146.6	146.6	152.5	150.2	152.1	151.6	152.5	150.8	145.4
1014	149.4	148.1	148.7	148.9	155.2	152.3	154.6	153.6	154.6	152.9	147.2
1013	152.8	150.8	151.1	151.6	157.5	154.4	157.1	155.8	156.6	156.2	150.7

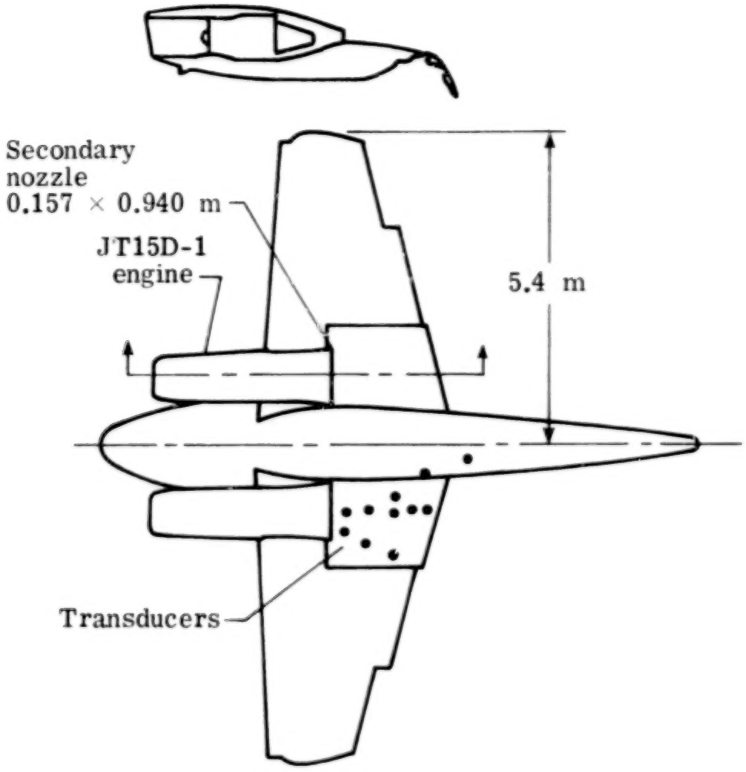

(a) Wind-tunnel model.

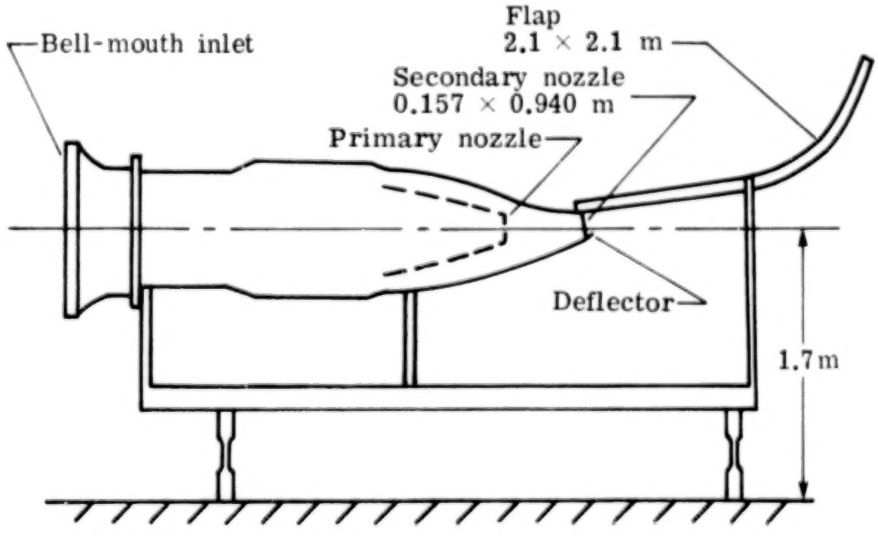

(b) Static model.

Figure 1.- Sketches of models.

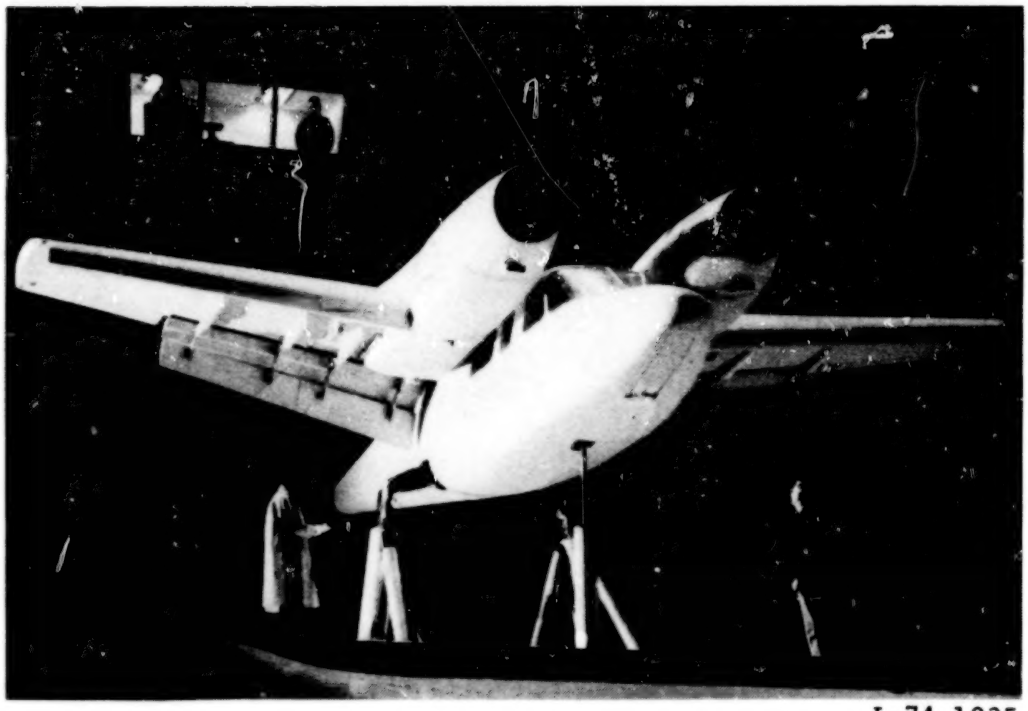

L-74-1835

(a) Wind-tunnel model.

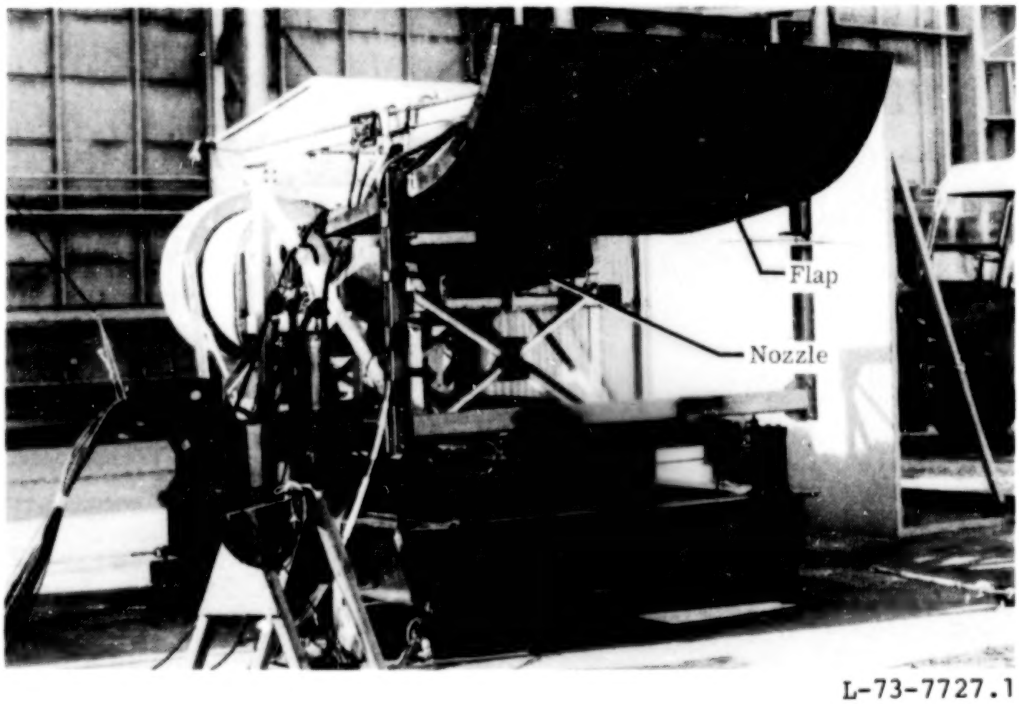

L-73-7727.1

(b) Static model without fuselage.

Figure 2.- Models.

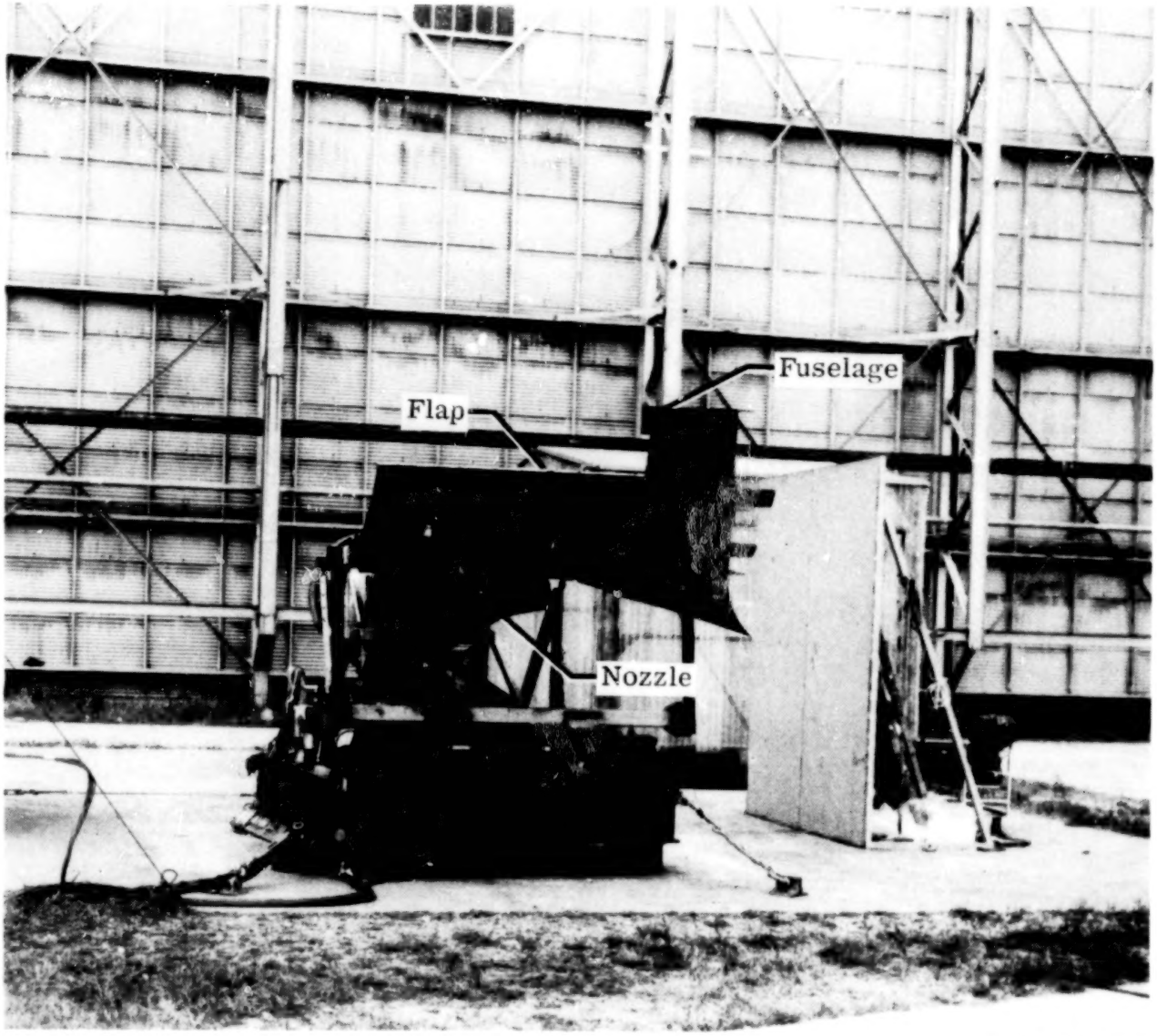

L-74-5883.1

(c) Static model with fuselage.

Figure 2.- Concluded.

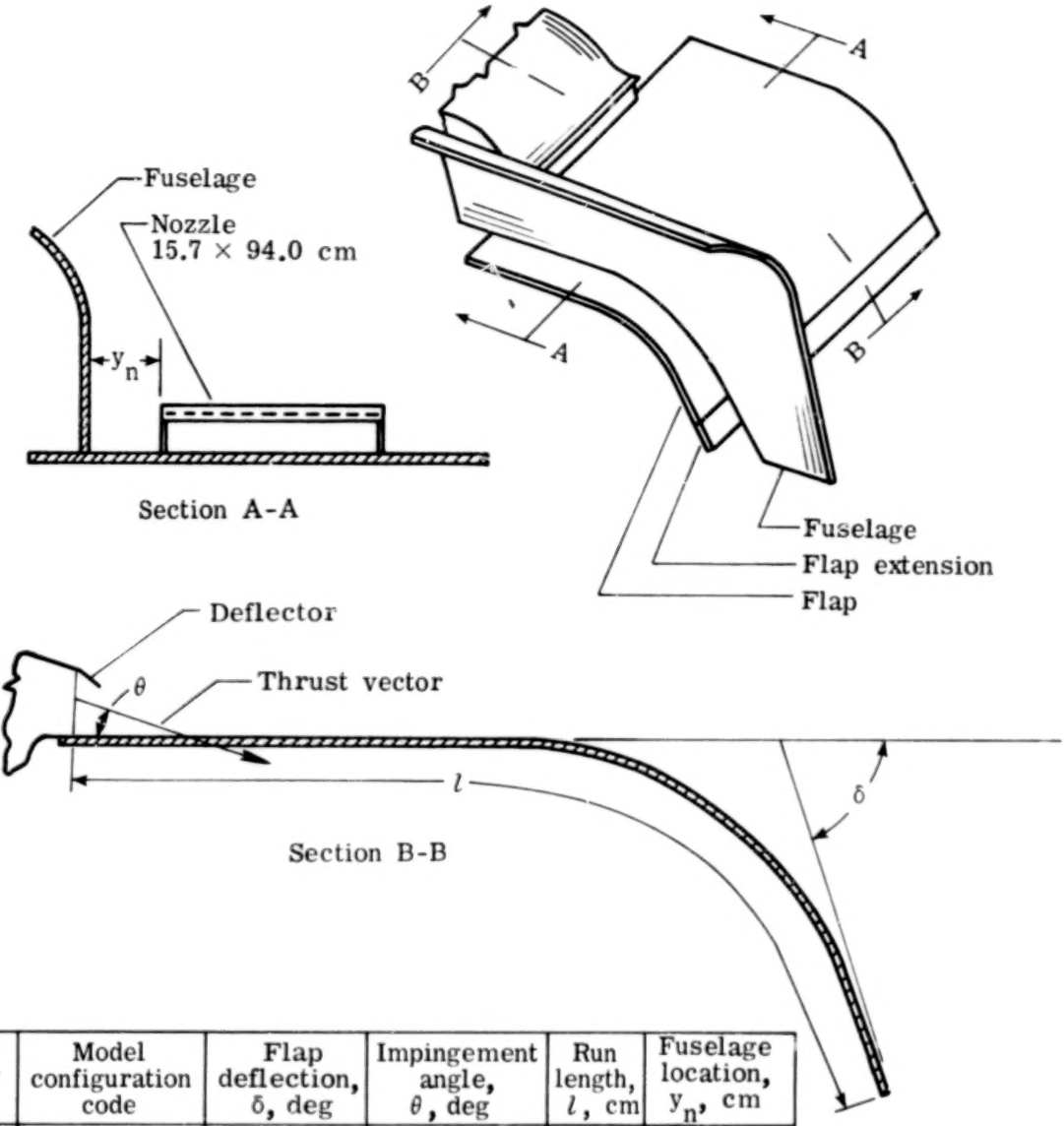

Model	Model configuration code	Flap deflection, δ, deg	Impingement angle, θ, deg	Run length, l, cm	Fuselage location, y_n, cm
Wind tunnel	1.1	32	5	199	10
	1.2	74	5	225	10
Static test stand	2.1	74	5	192	Removed
	2.2	74	5	192	1
	2.3	74	5	192	30
	2.4	74	5	192	60
	2.5	74	5	213	Removed
	2.6	74	11	192	Removed
	2.7	74	11	192	1
	2.8	74	11	213	Removed

(a) Configuration description.

Figure 3.- Flap and nozzle geometry.

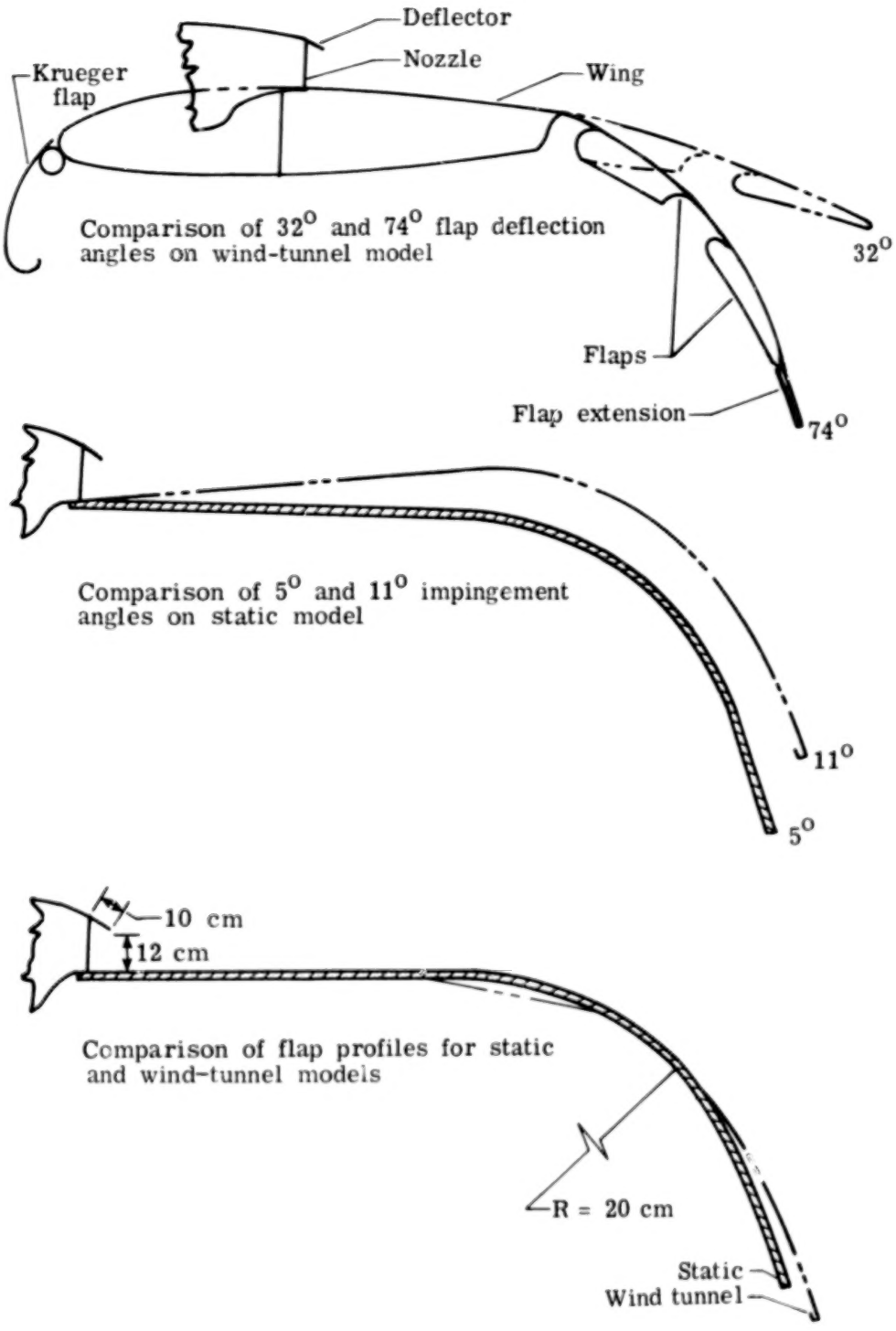

(b) Comparisons of flap contours.

Figure 3.- Concluded.

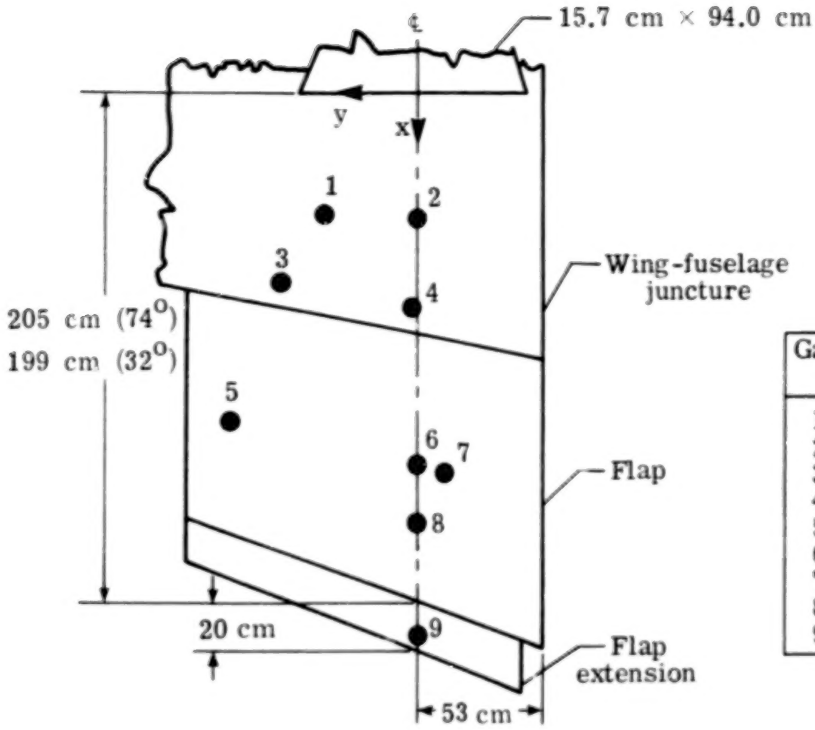

Gage	x, cm	y, cm
1	48	38
2	52	0
3	76	56
4	86	2
5	132	76
6	150	0
7	152	-10
8	181	0
9	218	0

(a) Wind-tunnel flaps.

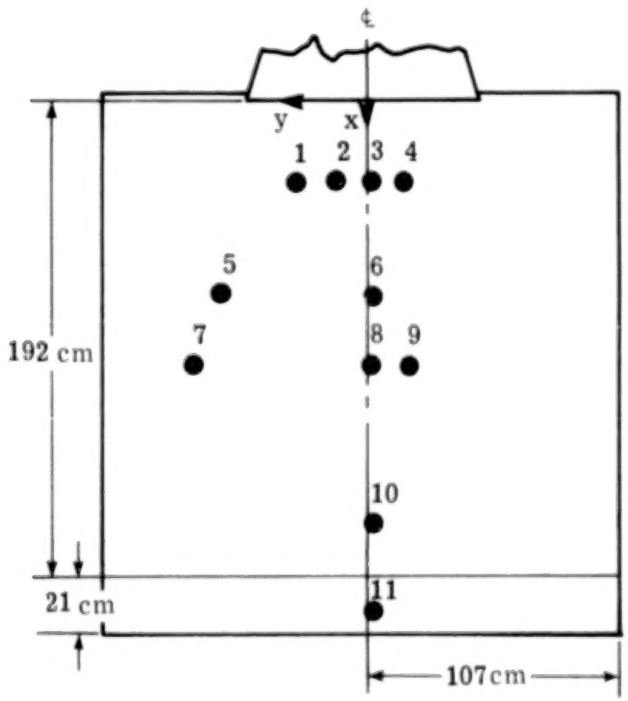

Gage	x, cm	y, cm
1	33	28
2	33	13
3	33	-3
4	33	-15
5	79	59
6	79	-3
7	107	69
8	107	-3
9	107	-18
10	170	-3
11	206	-3

(b) Static-test flaps.

Figure 4.- Transducer locations and flat pattern measurements along airfoil surface.

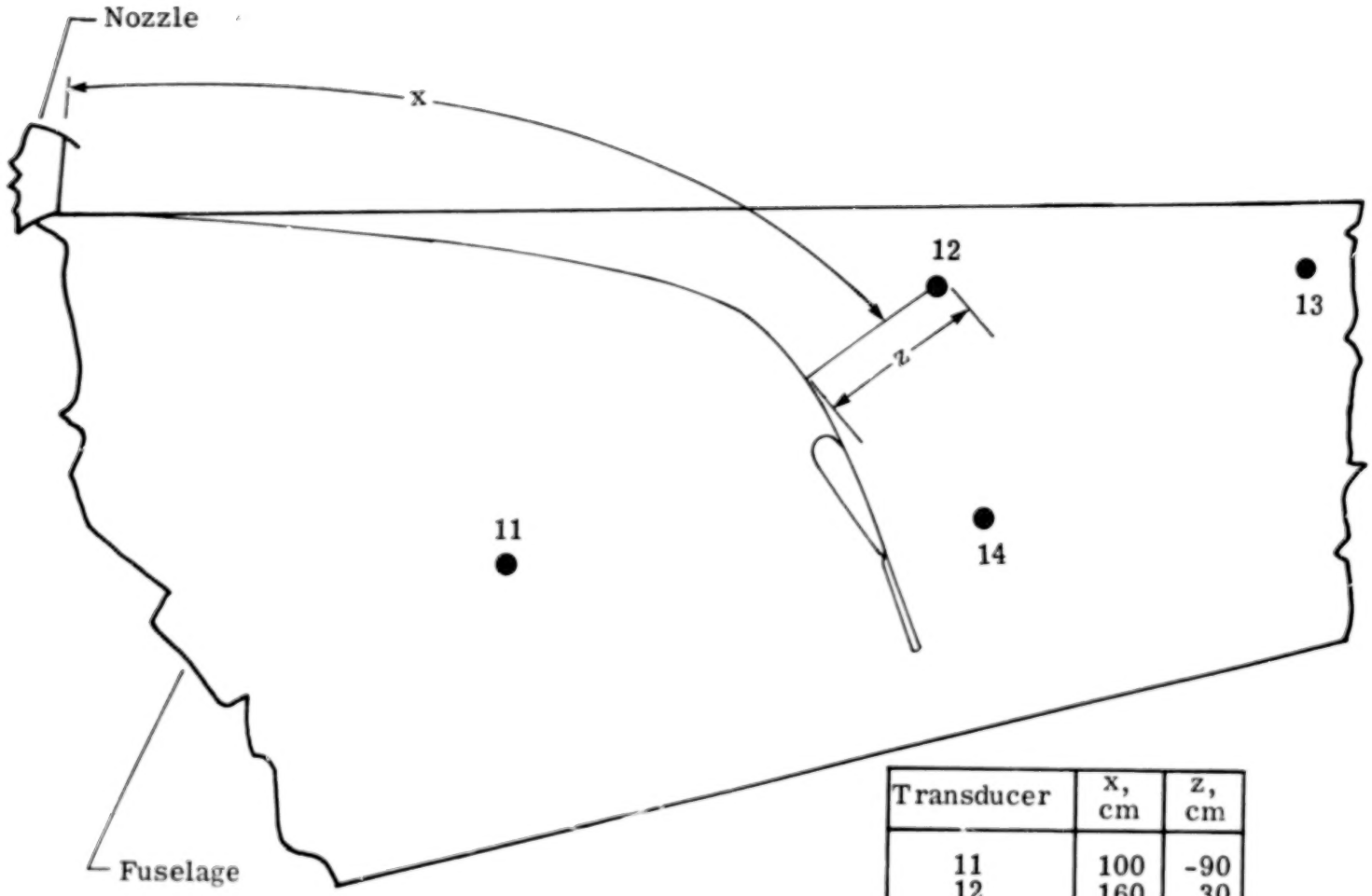

Transducer	x, cm	z, cm
11	100	-90
12	160	30
13	190	20
14	200	100

(c) Fuselage transducers.

Figure 4.- Concluded.

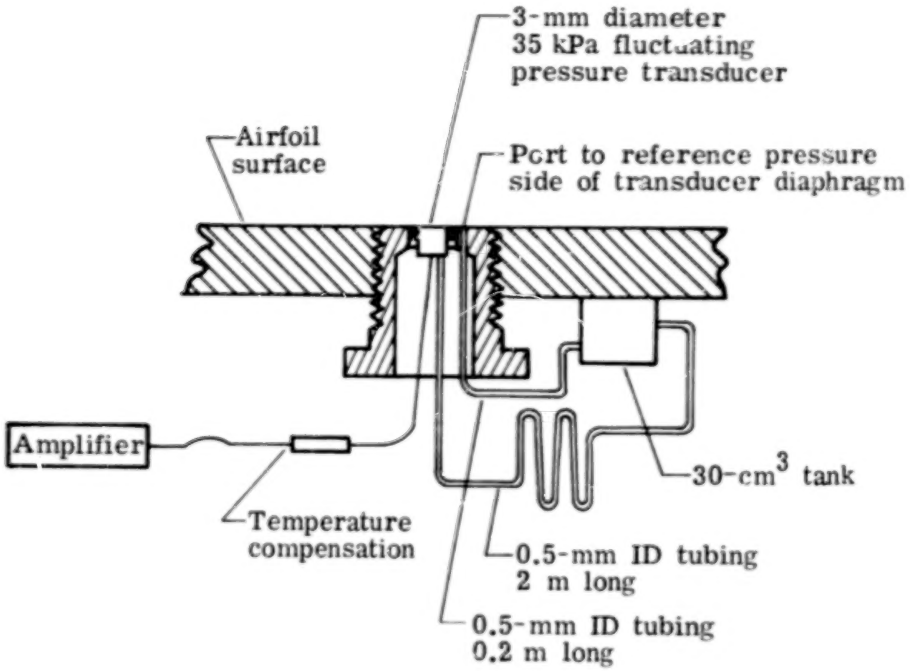

Figure 5.- Transducer installation detail.

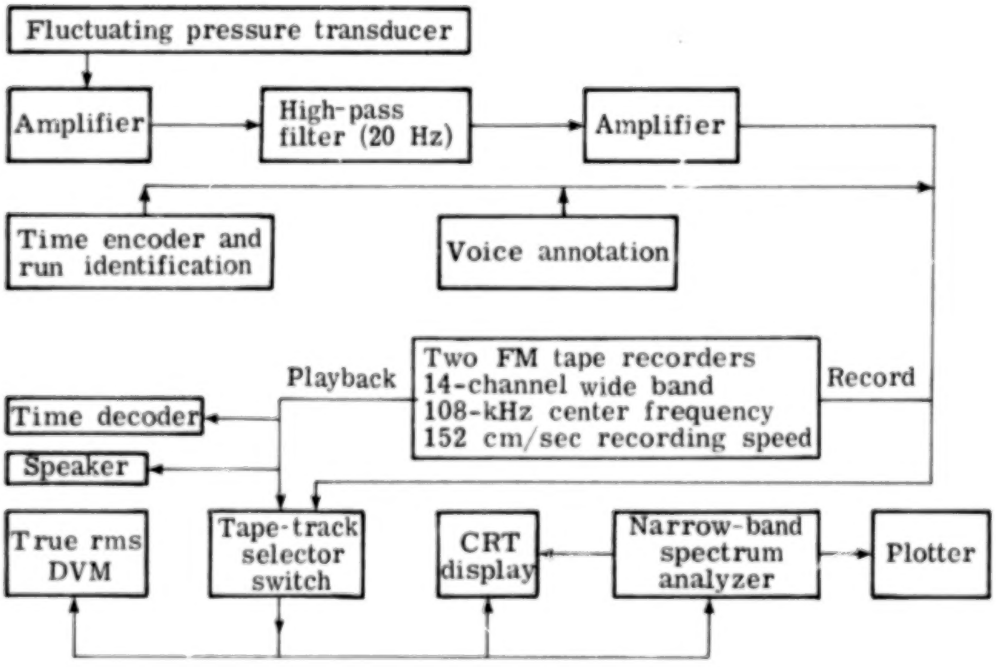

Figure 6.- Instrumentation schematic.

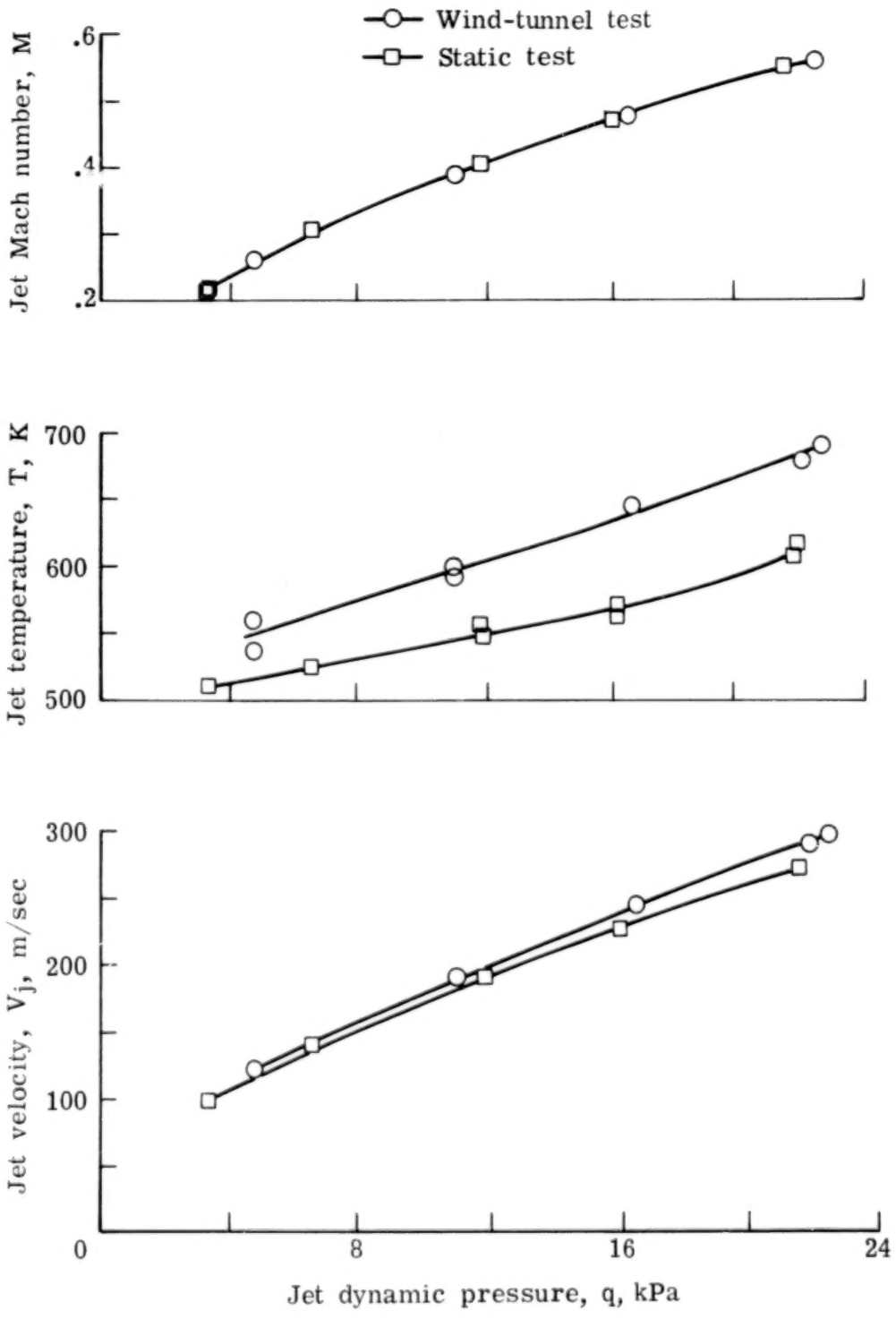

Figure 7.- Condition of efflux at jet exit.

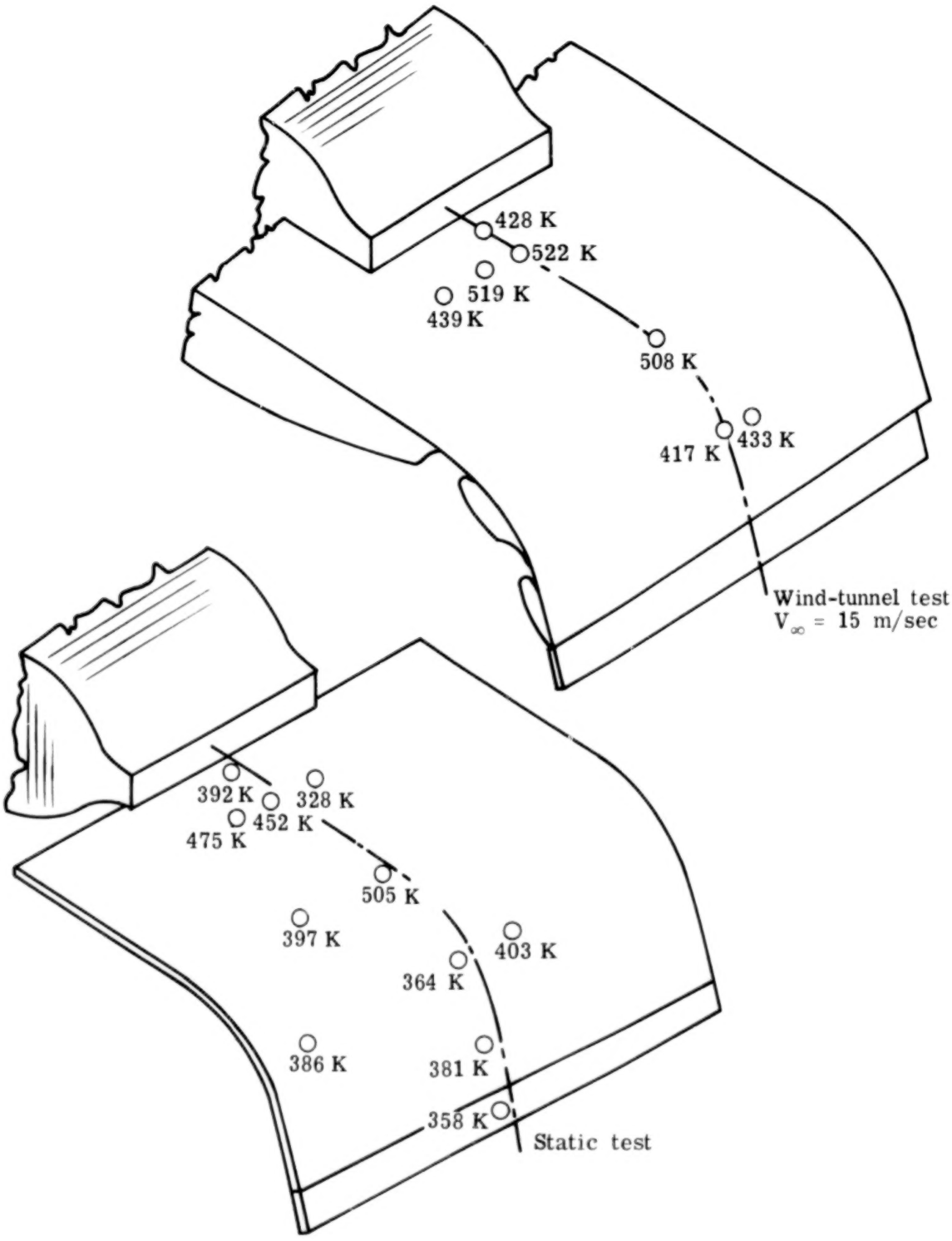

Figure 8.- Surface temperatures on flaps at q = 22 kPa.

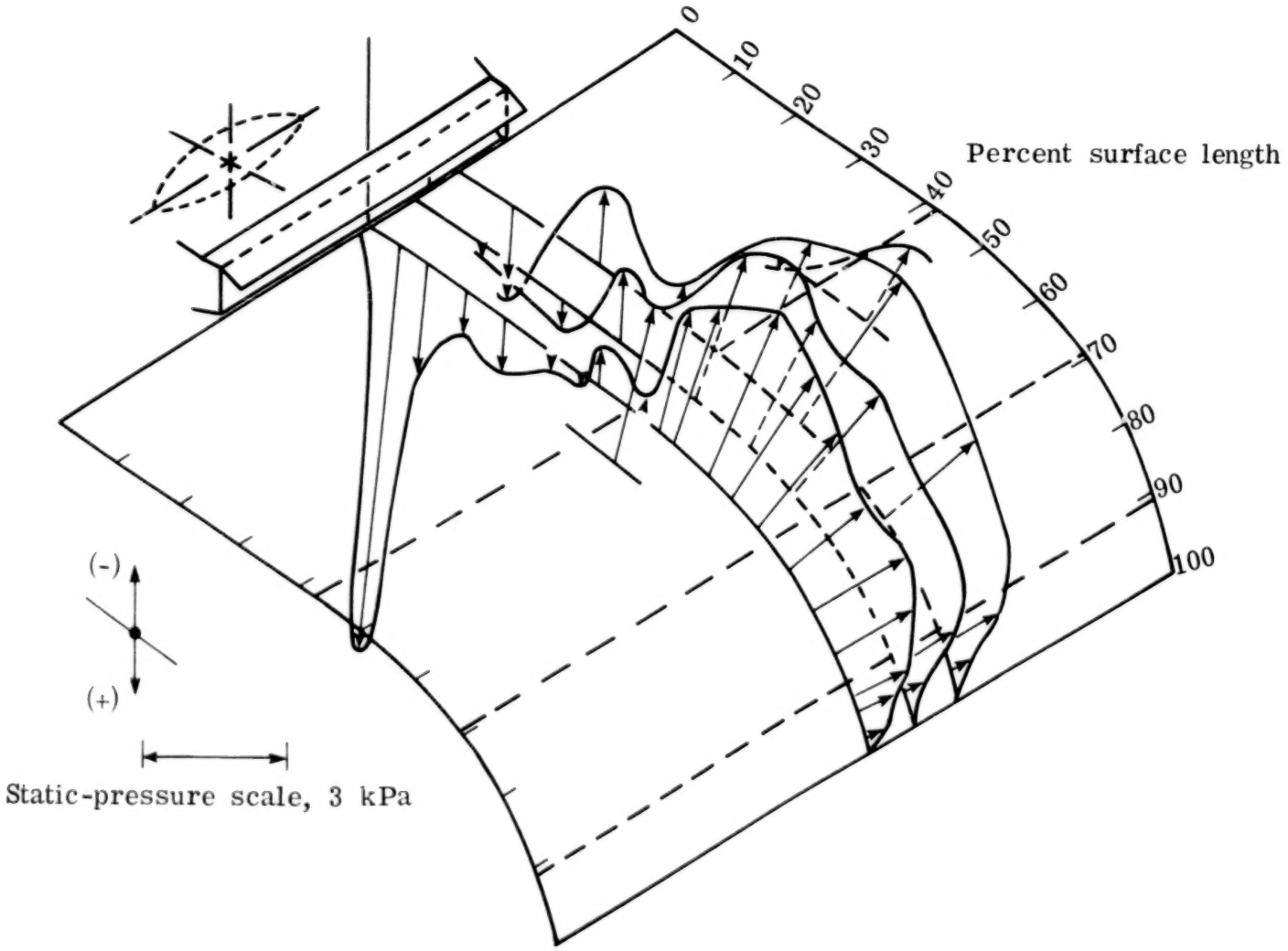

Figure 9.- Static gage pressure distribution on flap for q = 22 kPa and V_∞ = 0.

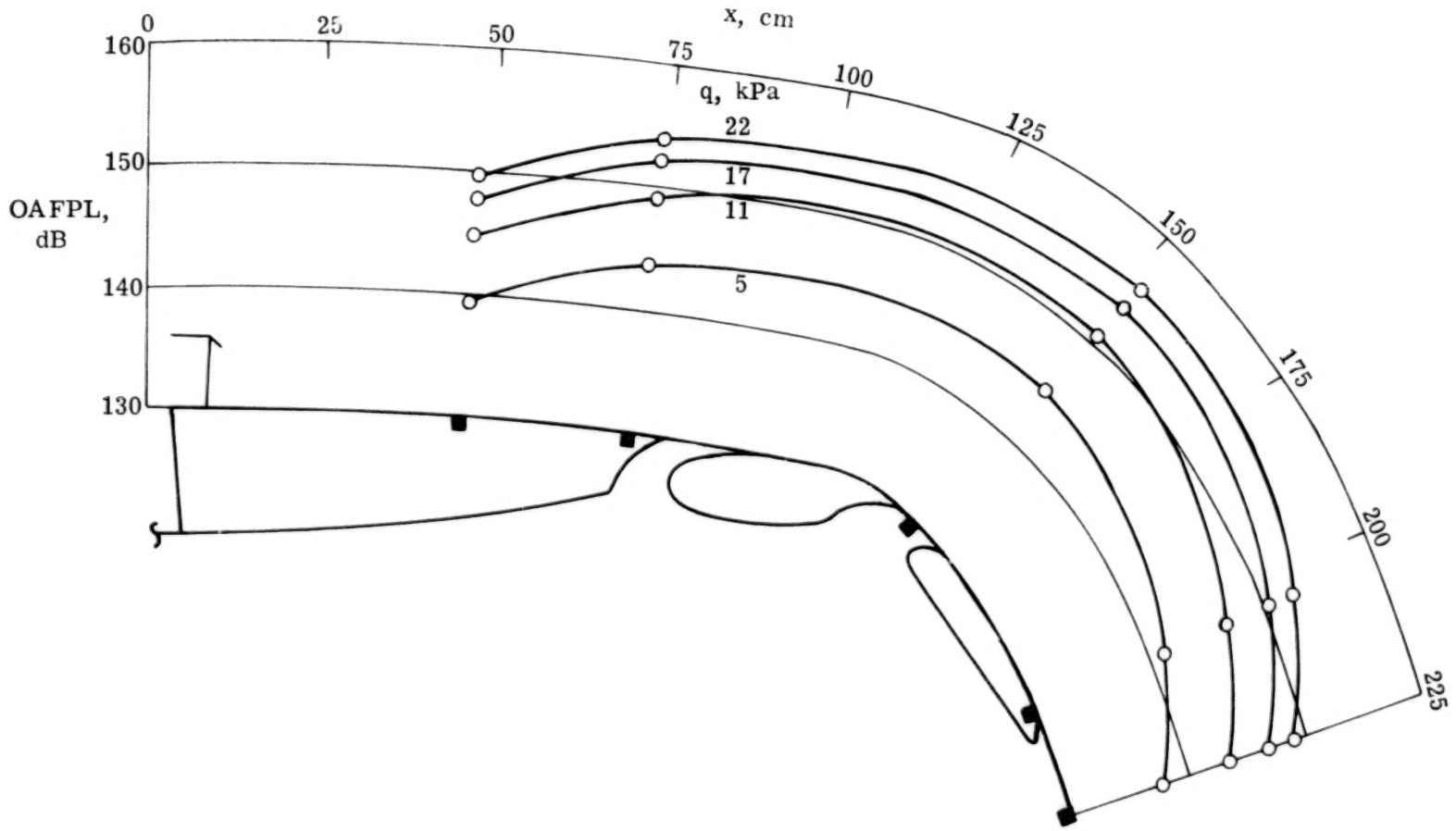

Figure 10.- OAFPL along center line of nozzle for four values of jet dynamic pressure. Configuration 1.2; $V_\infty = 0$.

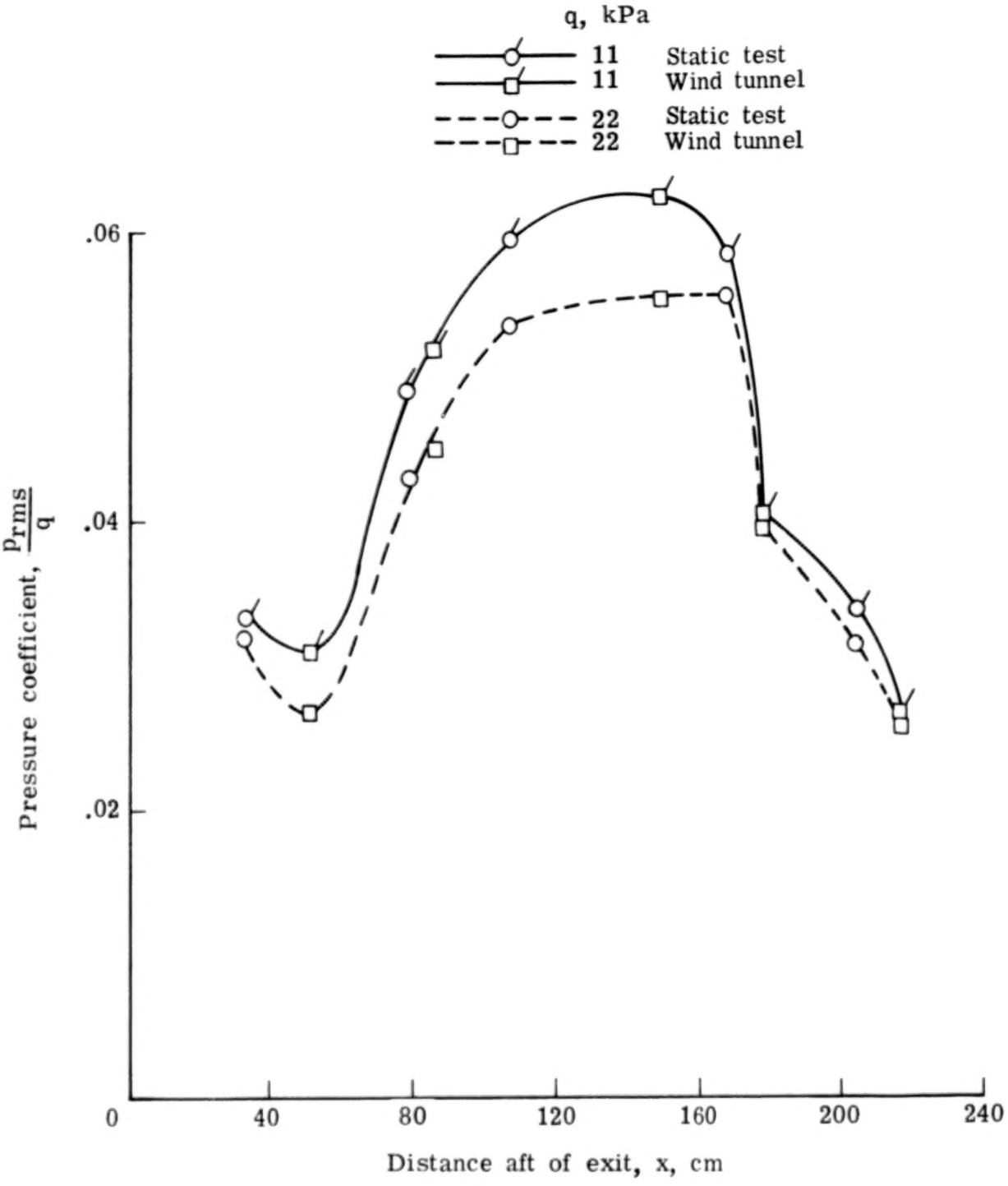

Figure 11.- Comparison of normalized fluctuating pressures on the flap for static and wind-tunnel tests for $V_\infty = 0$.

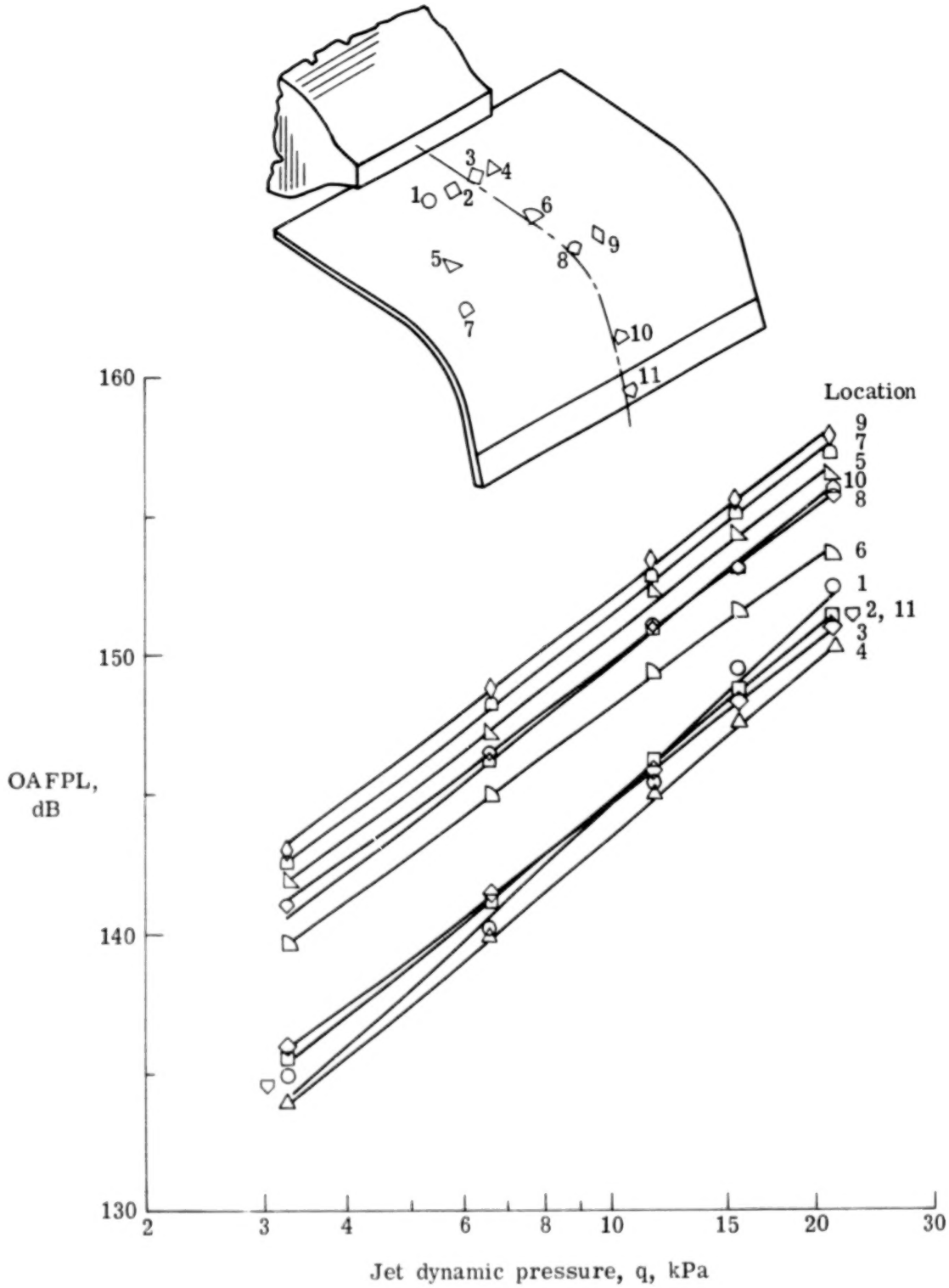

(a) OAFPL.

Figure 12.- Variation of flap loads with jet dynamic pressure.

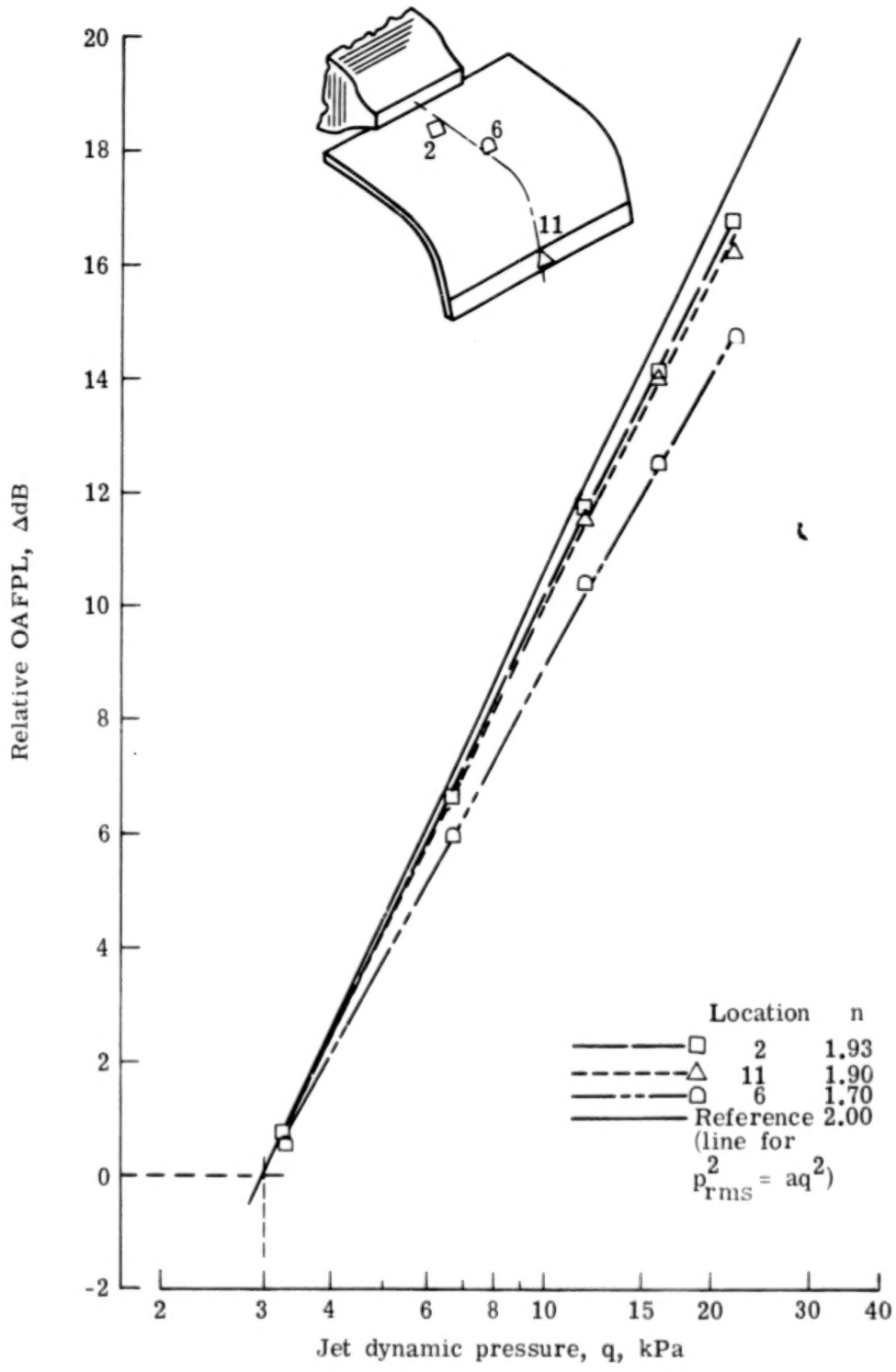

(b) Comparison of slopes.

Figure 12.- Concluded.

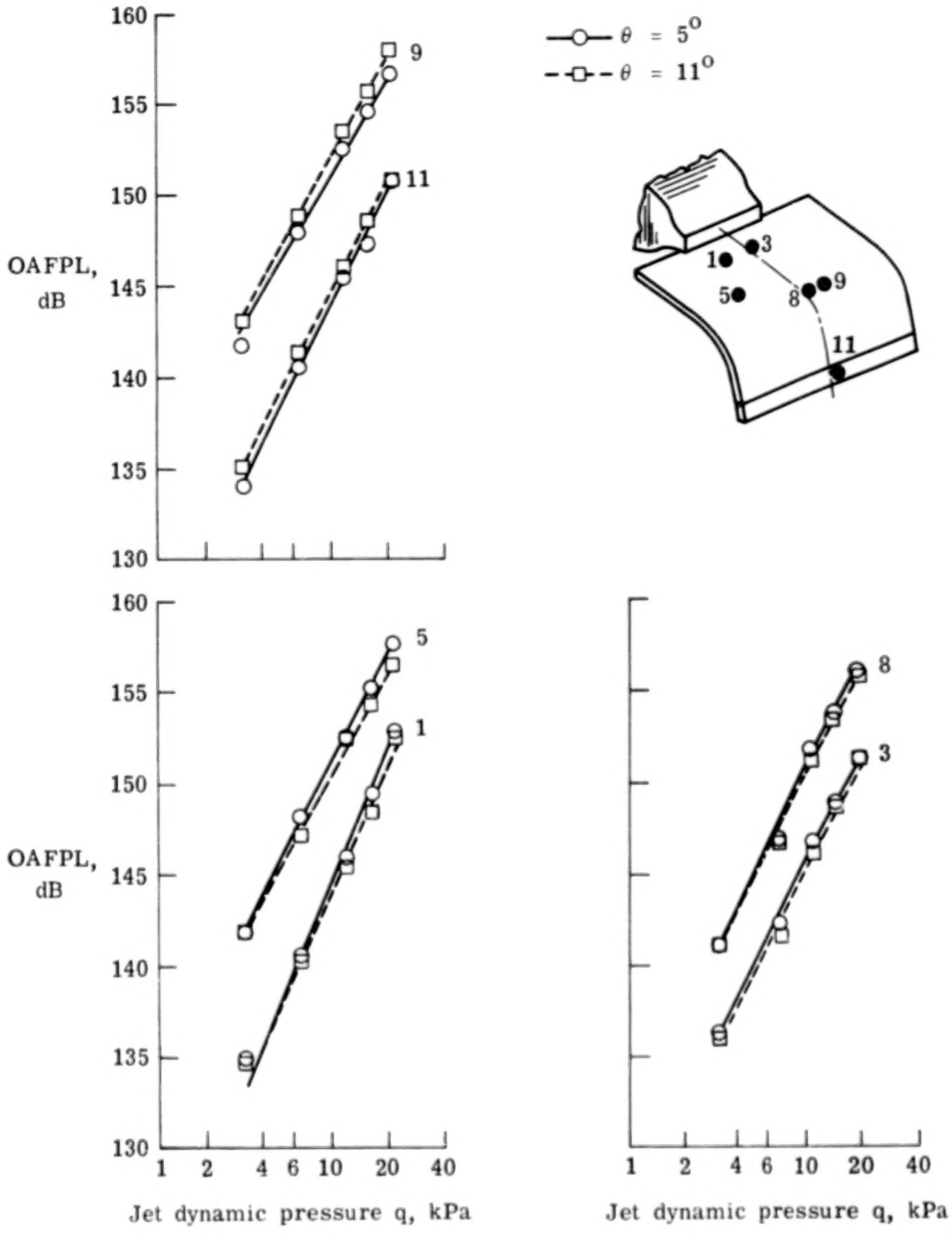

Figure 13.- Effect of jet impingement angle on OAFPL.

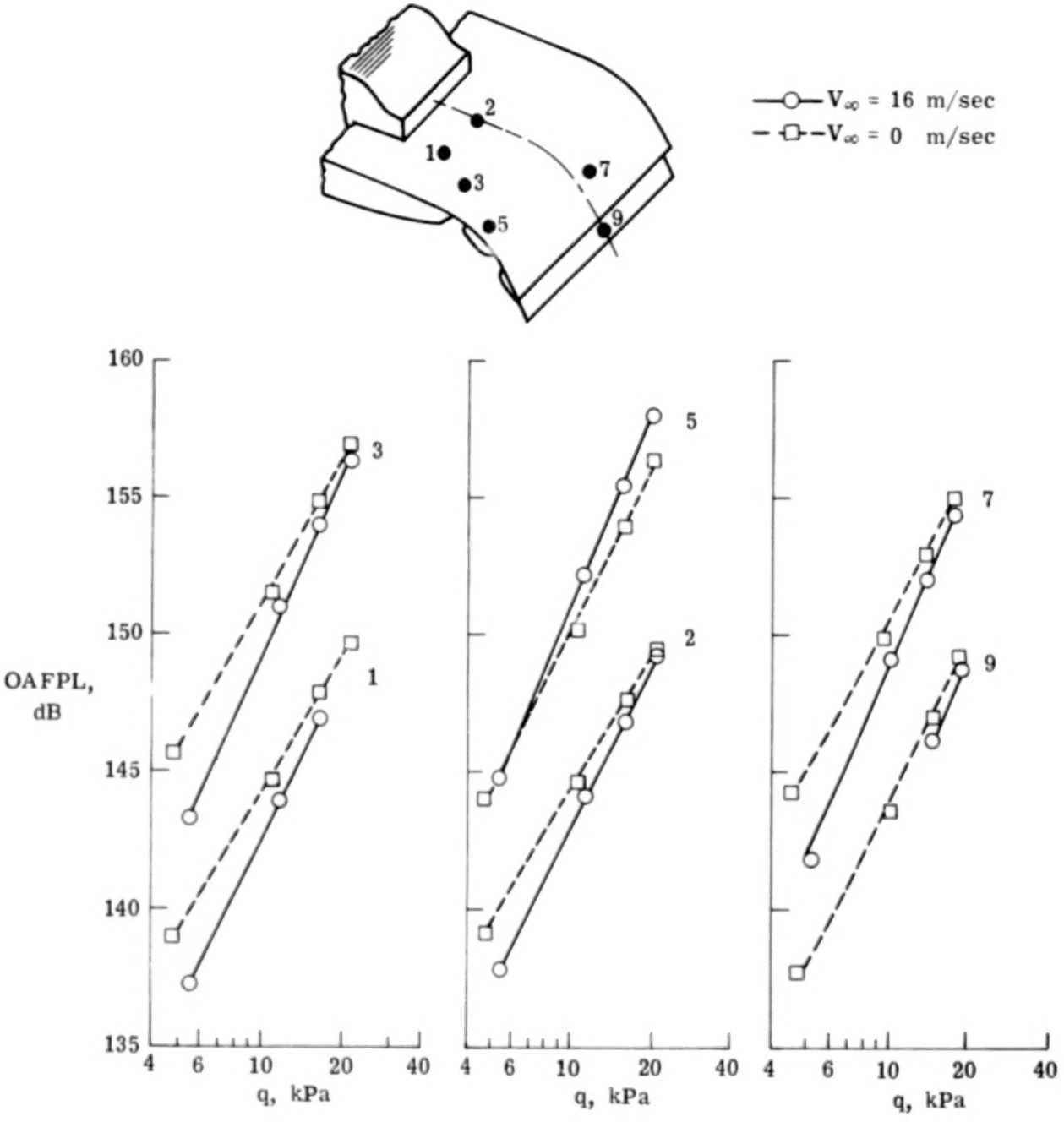

(a) Comparison of flap loads for $V_\infty = 0$ and $V_\infty = 16$ m/sec.

Figure 14.- Effect of airspeed on OAFPL.

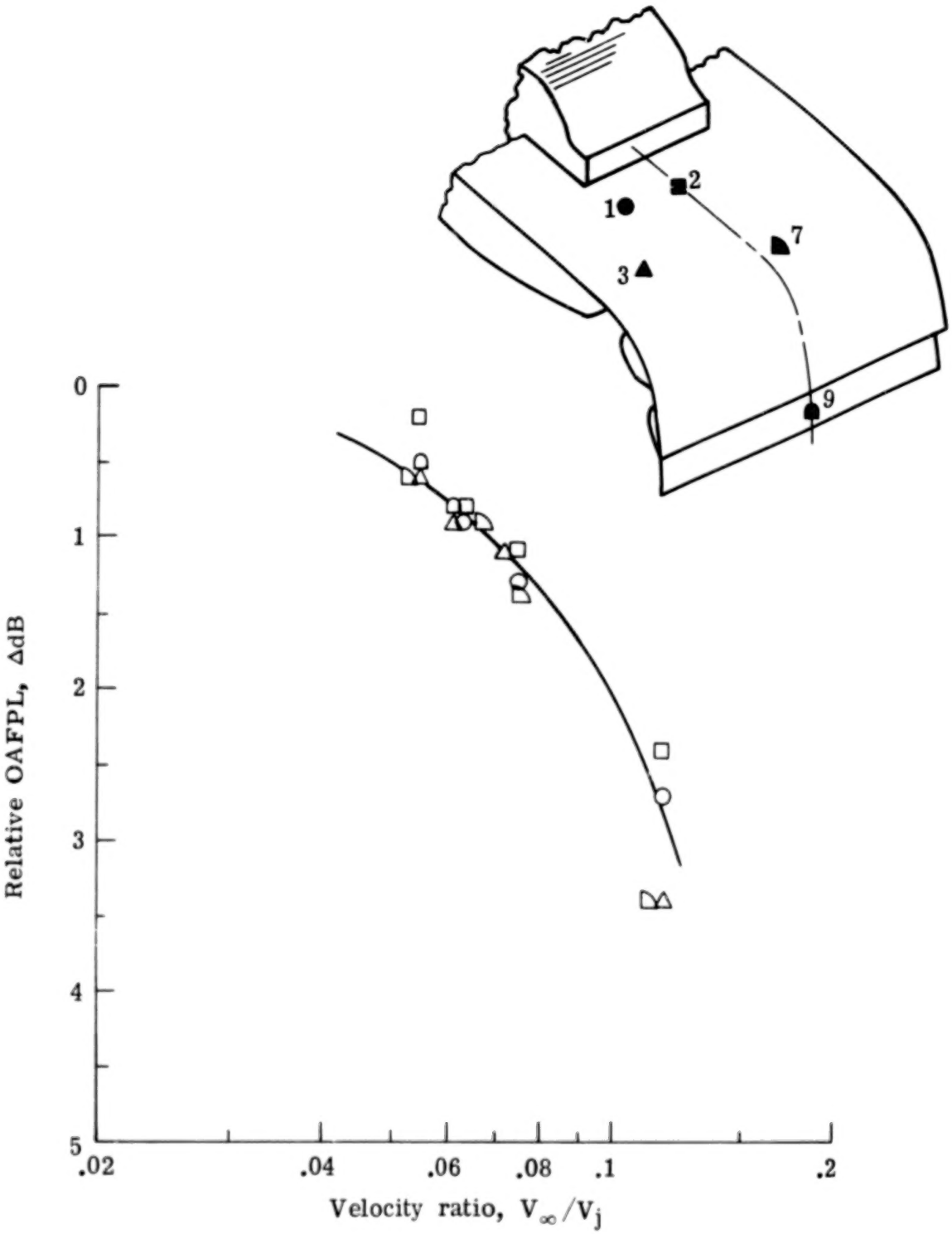

(b) Variation of flap loads with airspeed velocity ratio.

Figure 14.- Concluded.

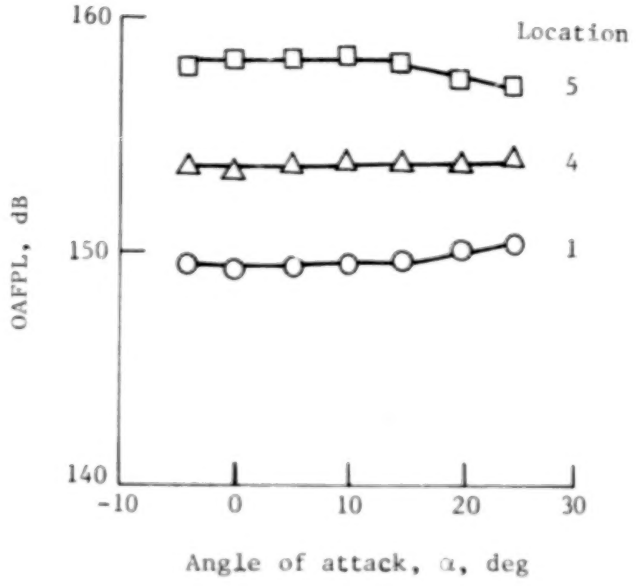

(a) Variation of OAFPL at three locations for V_∞ = 15 m/sec.

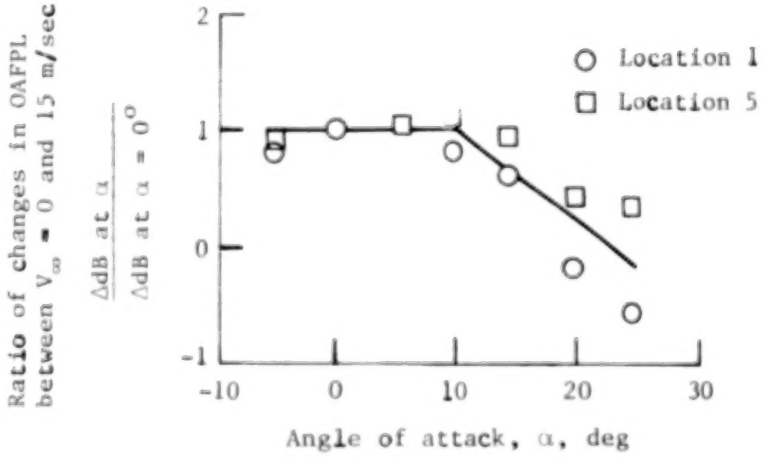

(b) Relative magnitude of airspeed effect.

Figure 15.- Effect of angle of attack on OAFPL.

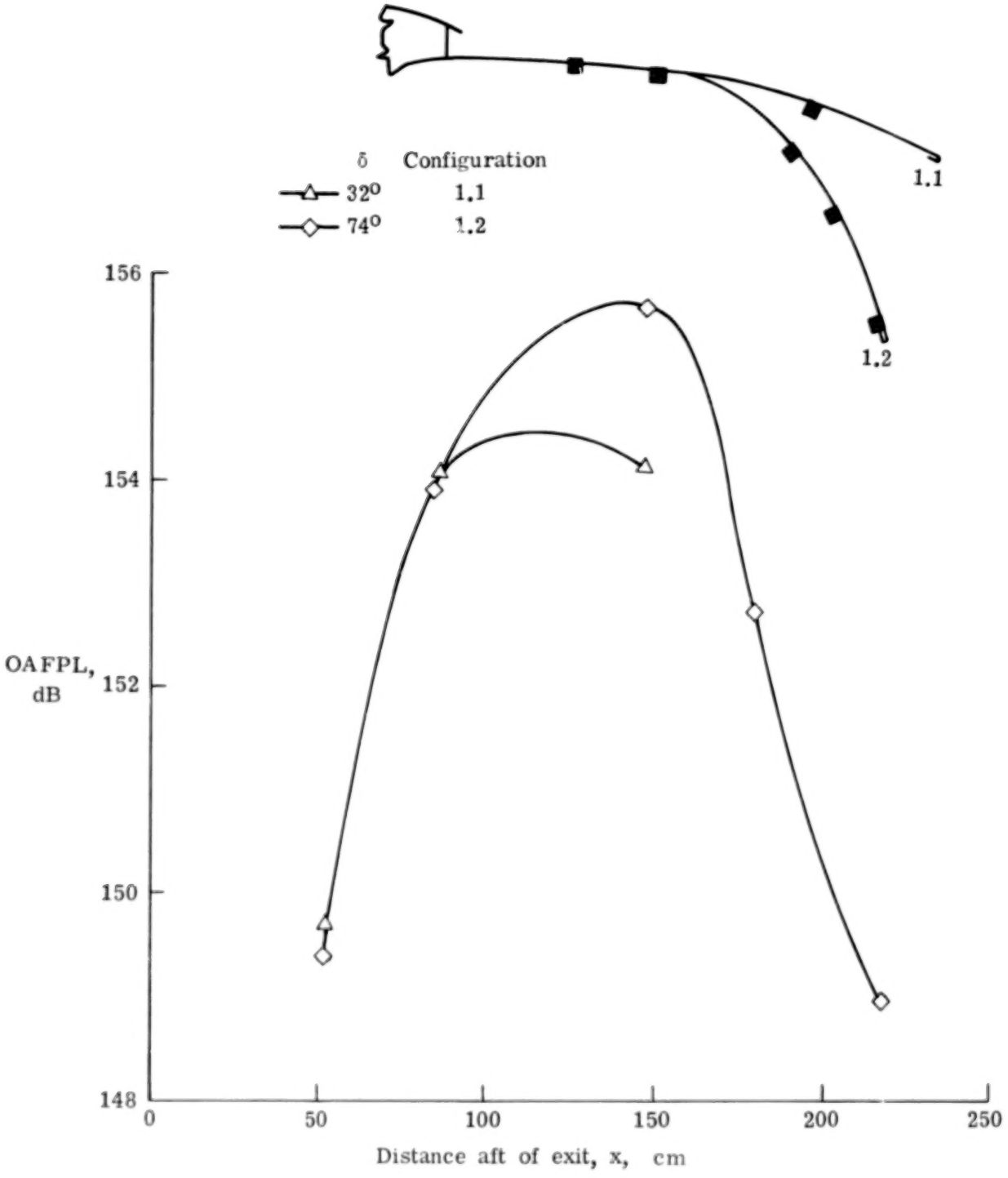

(a) Loads along nozzle center line for $V_\infty = 0$ and $q = 22$ kPa.

Figure 16.- Comparison of loads on 32° and 74° flaps.

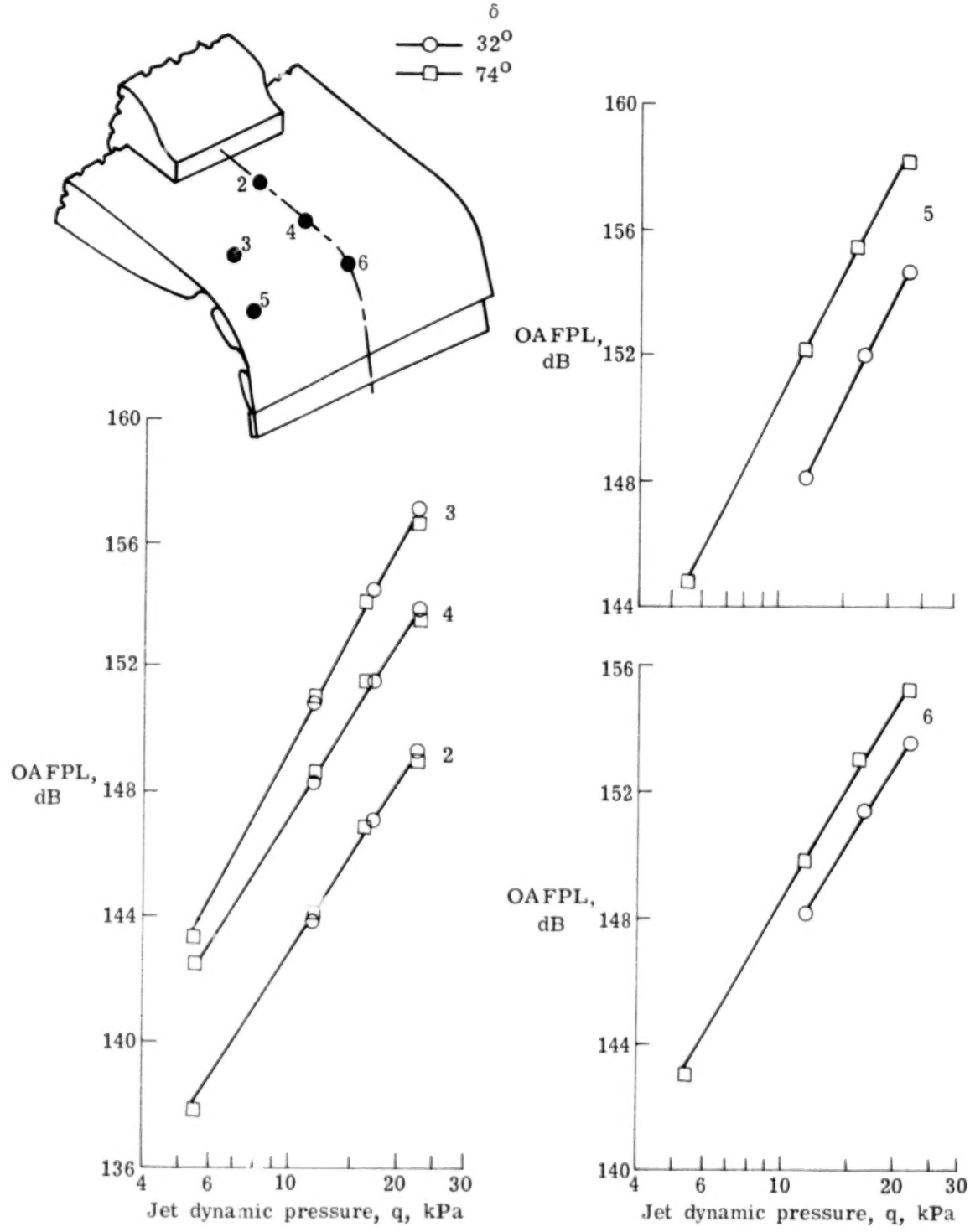

(b) Variation in loading with dynamic pressure for V_∞ = 16 m/sec.

Figure 16.- Concluded.

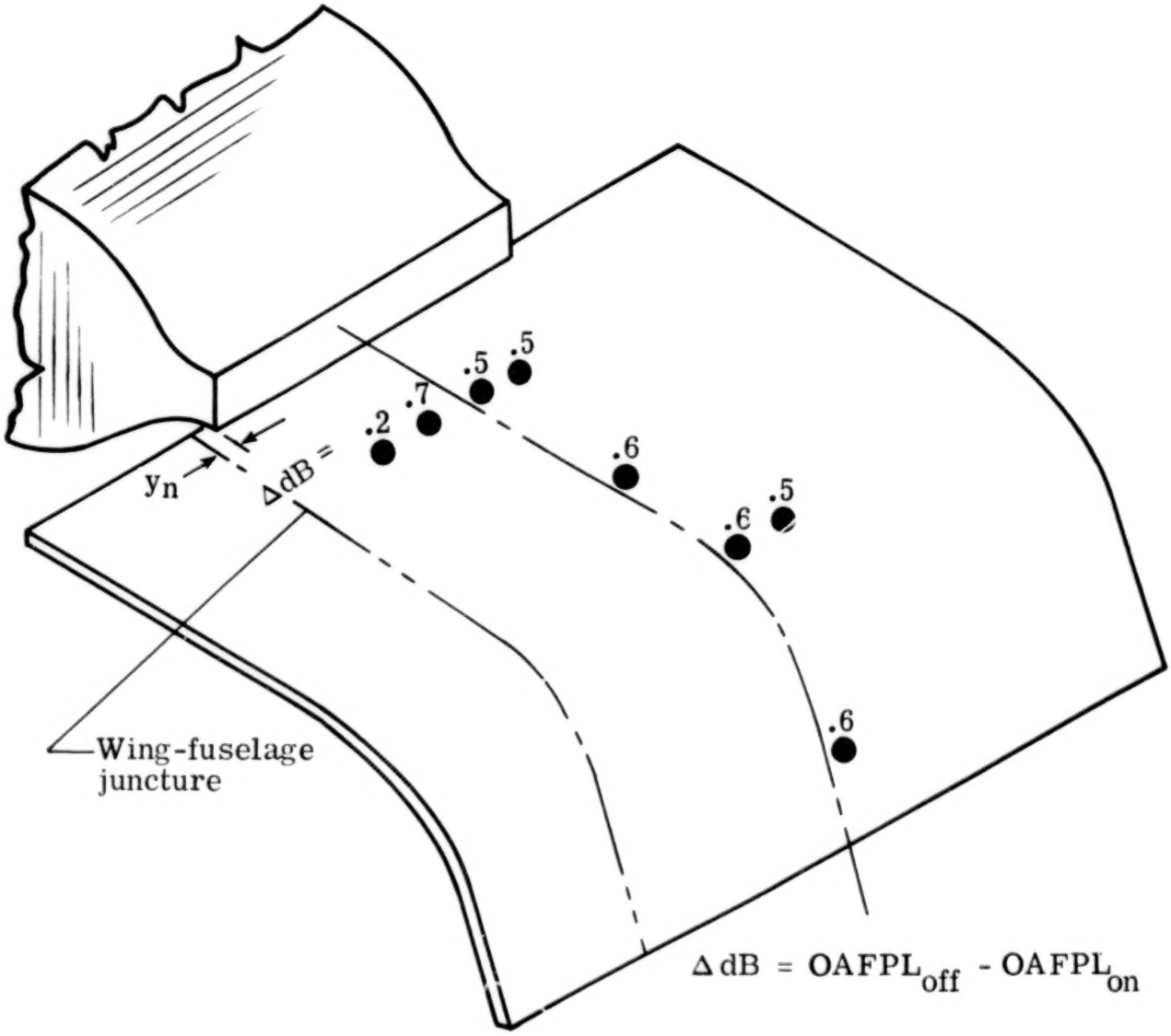

(a) Decrease in flap loads for installation of fuselage at y_n = 1 cm for q = 22 kPa.

Figure 17.- Effect of engine-fuselage location on flap loads.

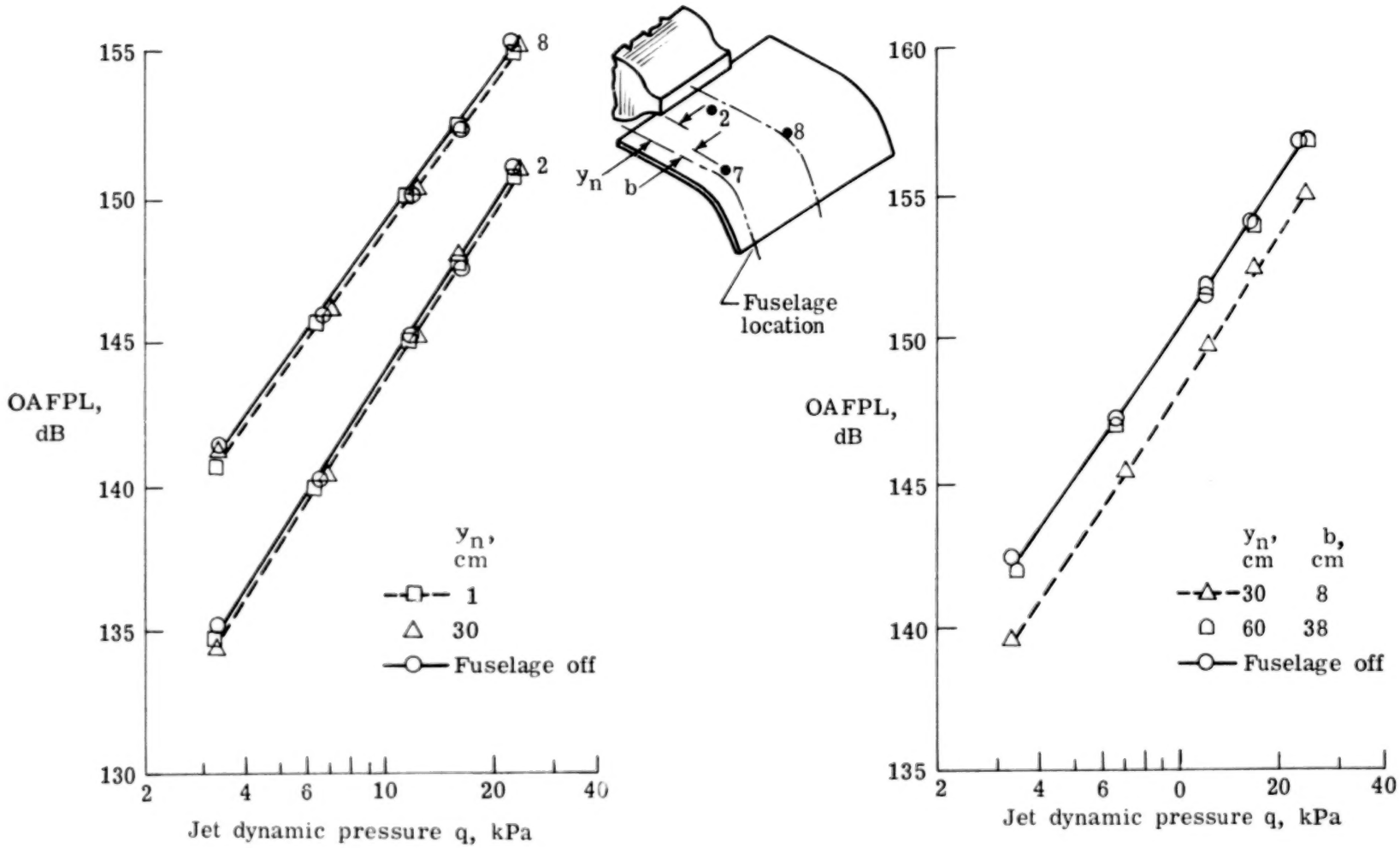

(b) Measurements far from fuselage (locations 2 and 8).

(c) Measurements near fuselage (location 7).

Figure 17.- Concluded.

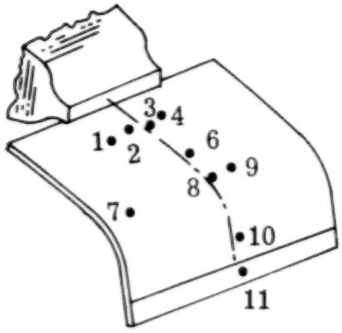

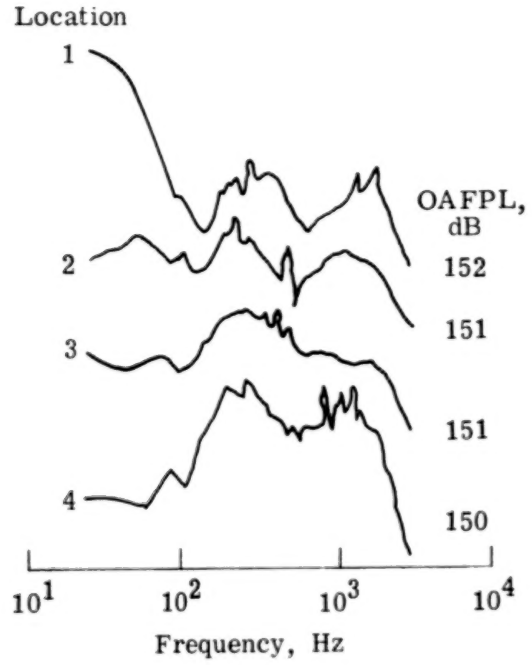

(a) Spectra for locations near nozzle exit.

(b) Spectra for locations on engine center line.

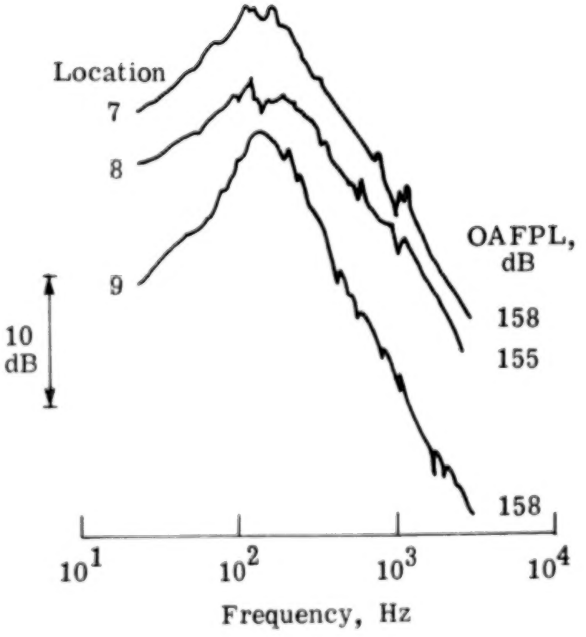

(c) Spectra for locations near flap knee.

Figure 18.- Comparison of spectra shapes of fluctuating pressure PSD for q = 22 kPa.

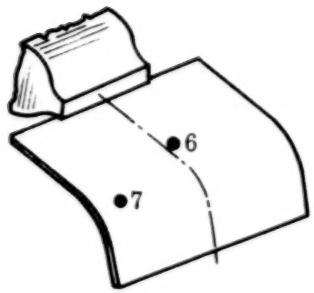

Jet-exit conditions		Spectrum parameters							
		Location 6				Location 7			
q, kPa	V_j, m/sec	OAFPL, dB	FPL_{max}, $(Pa)^2$	f_{max}, Hz	Roll-off, dB/octave	OAFPL, dB	FPL_{max}, $(Pa)^2$	f_{max}, Hz	Roll-off, dB/octave
3.3	98	140	30	90	5	142	50	60	5
6.5	139	144	60	130	5-1/2	147	150	110	5-1/2
11.7	192	149	180	170	5-1/2	152	340	100	5-1/2
16.0	226	150	230	180	5-1/2	154	430	170	6
22.2	276	153	290	270	5-1/2	157	670	200	5-1/2

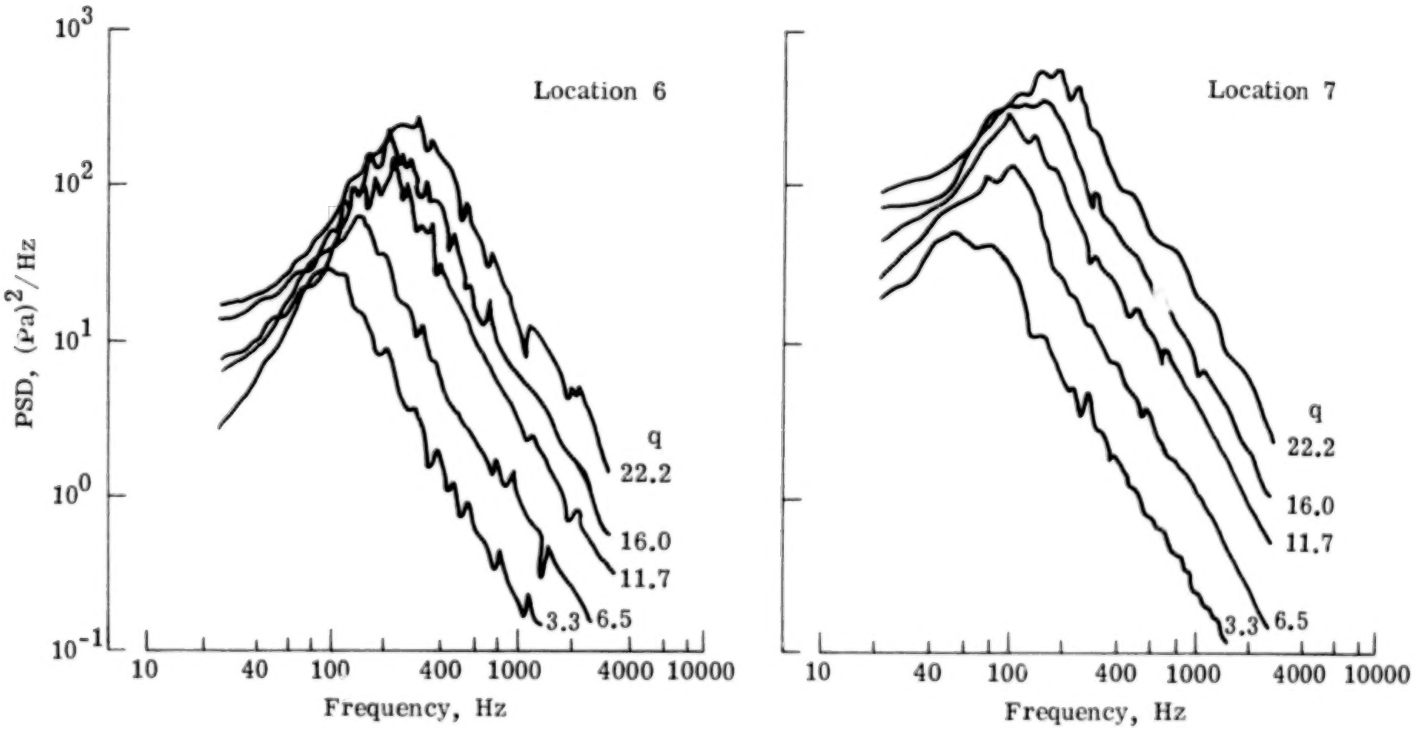

Figure 19.- Variation in PSD with jet dynamic pressure.

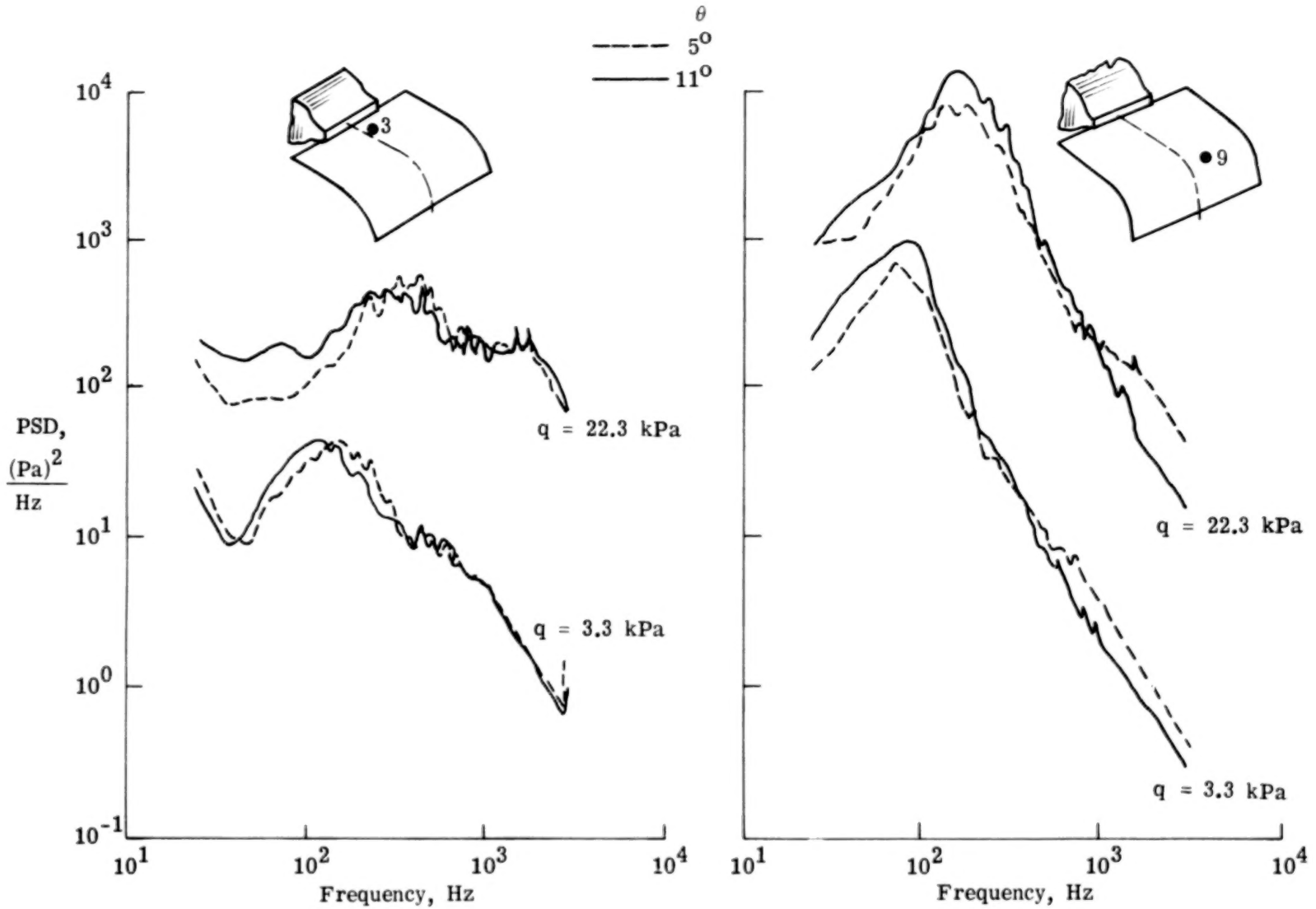

Figure 20.- Comparison of PSD for 5° and 11° impingement angles.

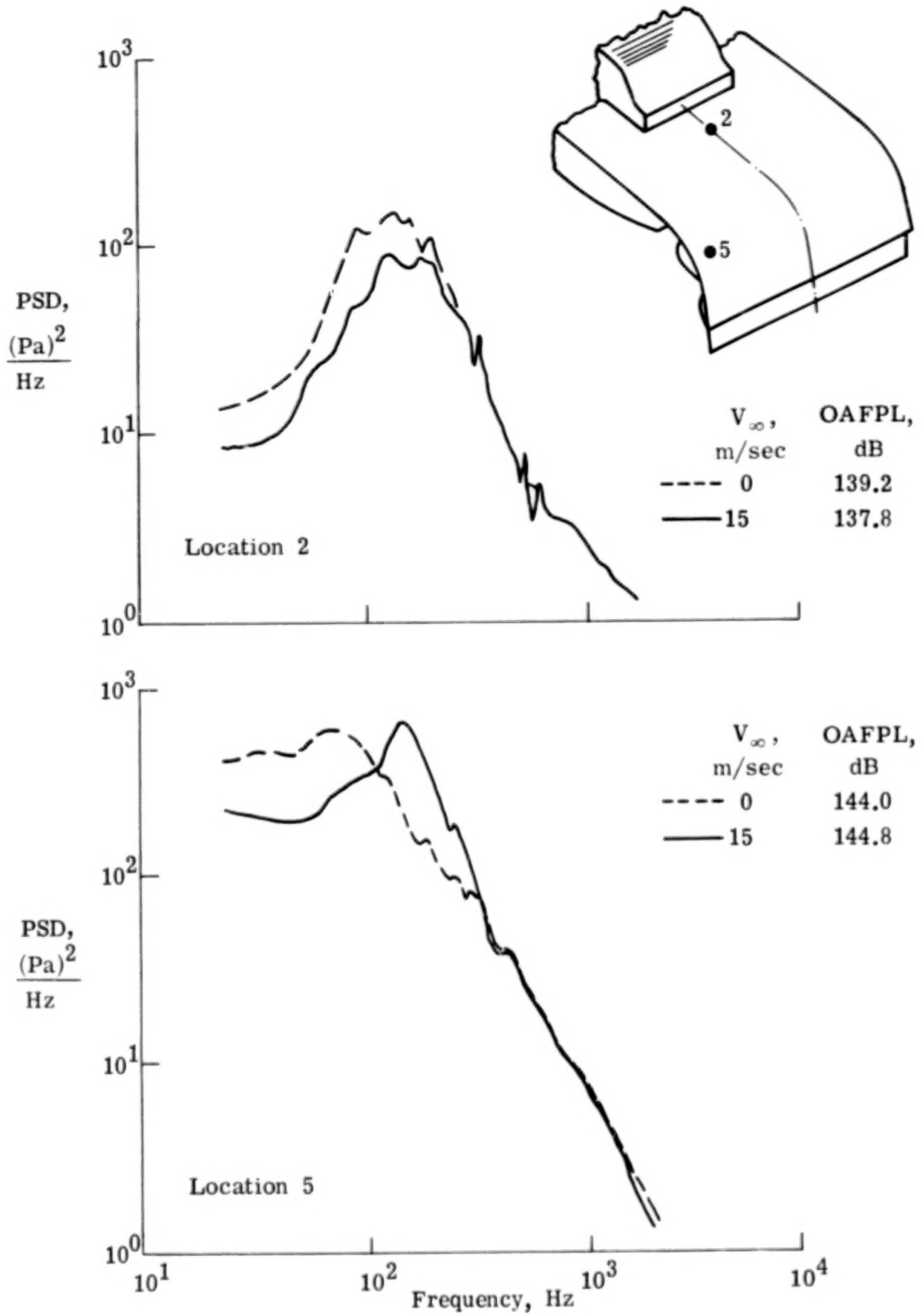

(a) q = 5 kPa.

Figure 21.- Comparison of PSD for airspeeds of V_∞ = 0 and 15 m/sec.

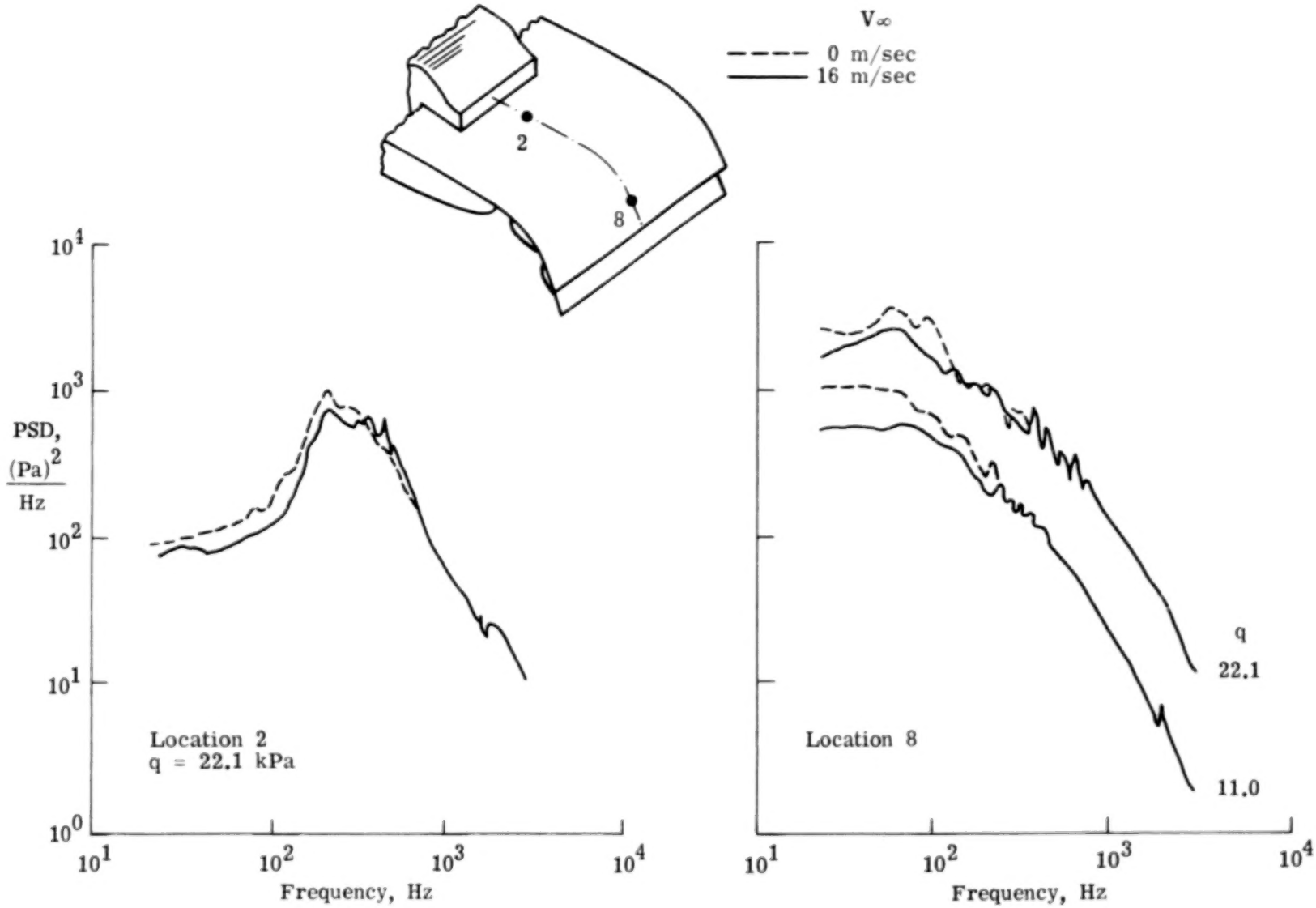

(b) q = 11 kPa and 22 kPa.

Figure 21.- Concluded.

45

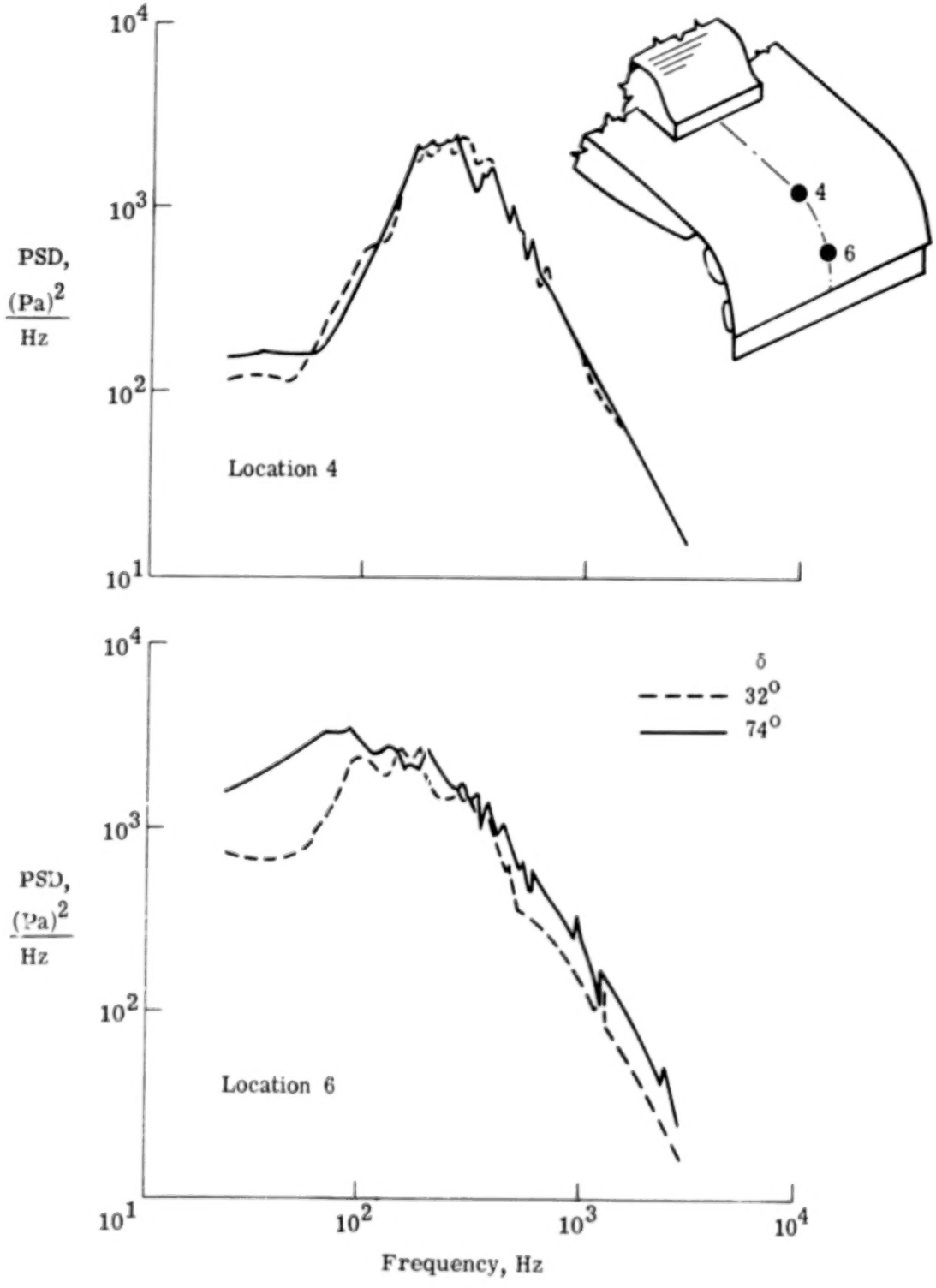

Figure 22.- Comparison of PSD for 32° and 74° flaps.

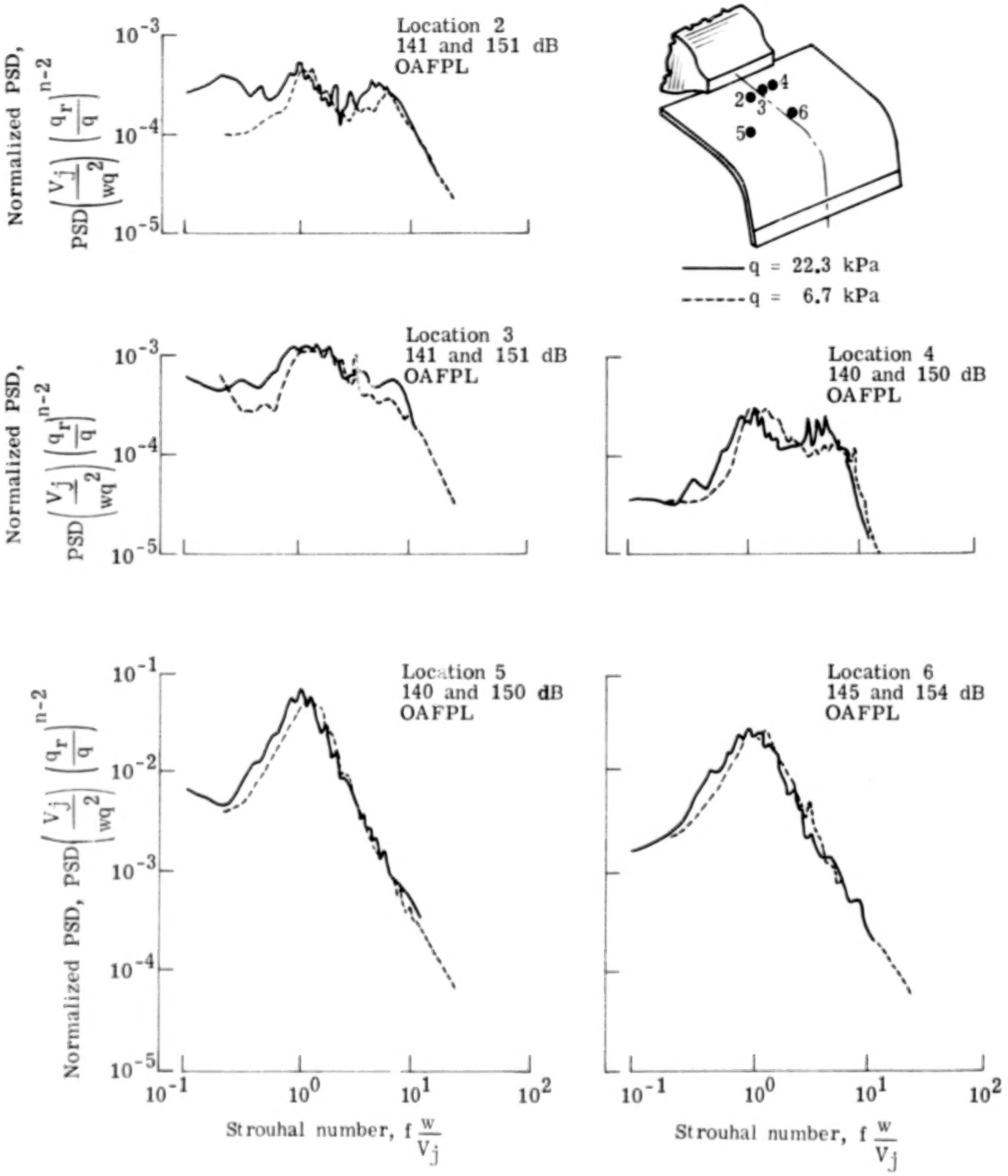

Figure 23.- Comparison of normalized flap loads spectra for q = 6.7 kPa and 22.3 kPa.

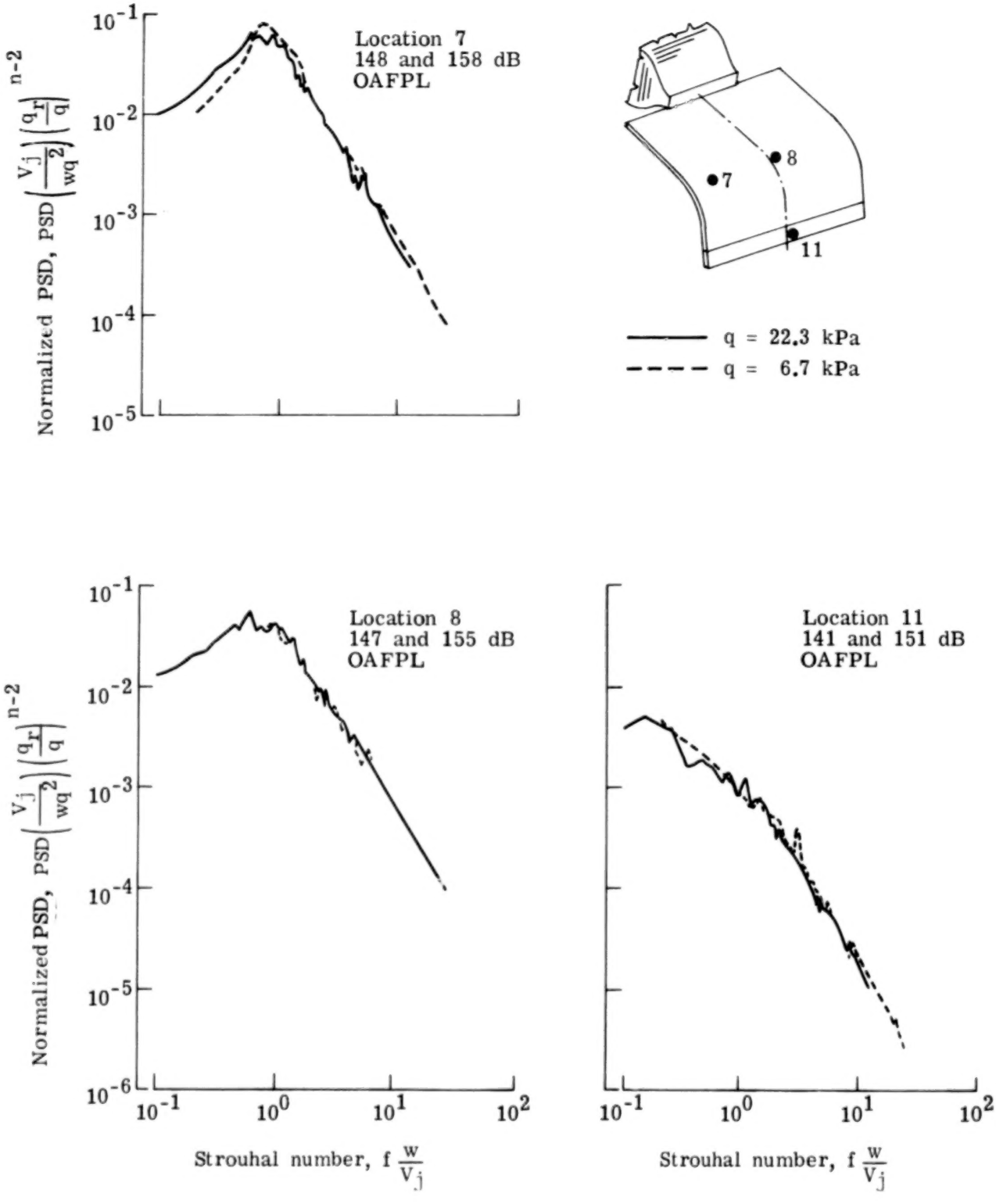

Figure 23.- Concluded.

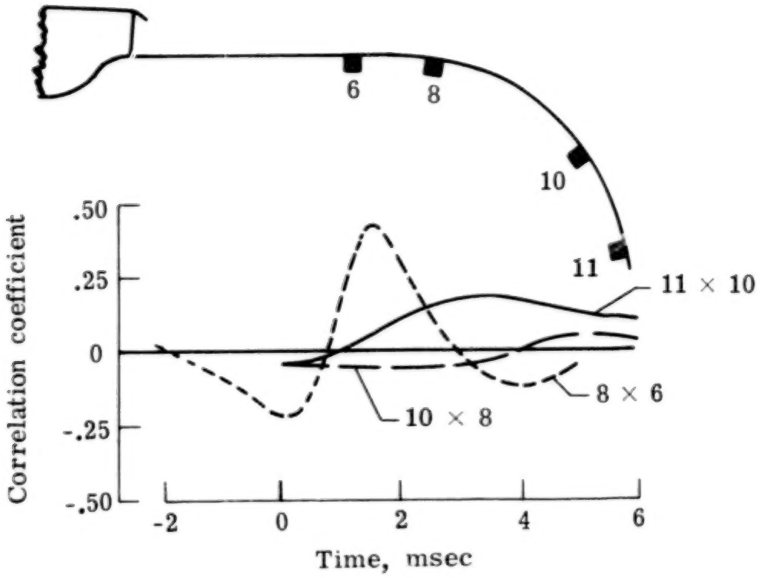

(a) Cross-correlation function for three sets of measurement locations. Configuration 2.5.

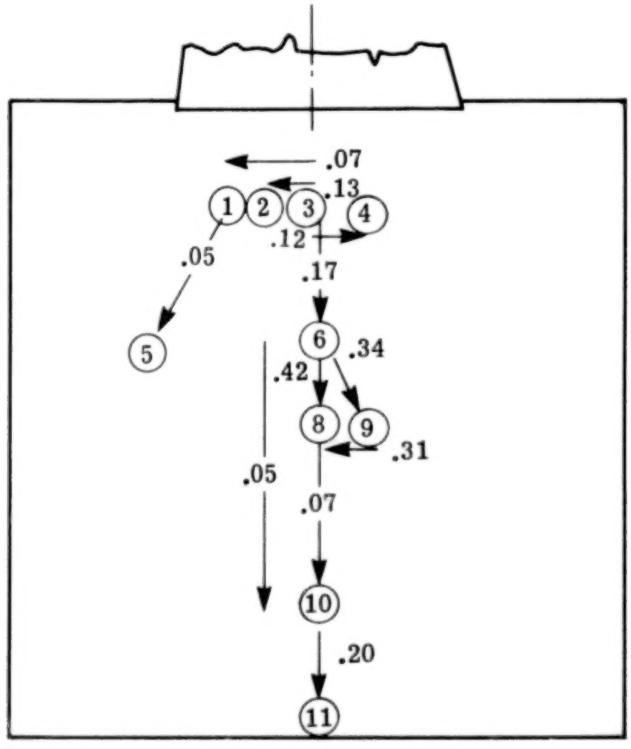

(b) Cross-correlation maximum coefficients for configuration 2.5.

Figure 24.- Cross-correlation coefficients of fluctuating pressures for q = 22 kPa.

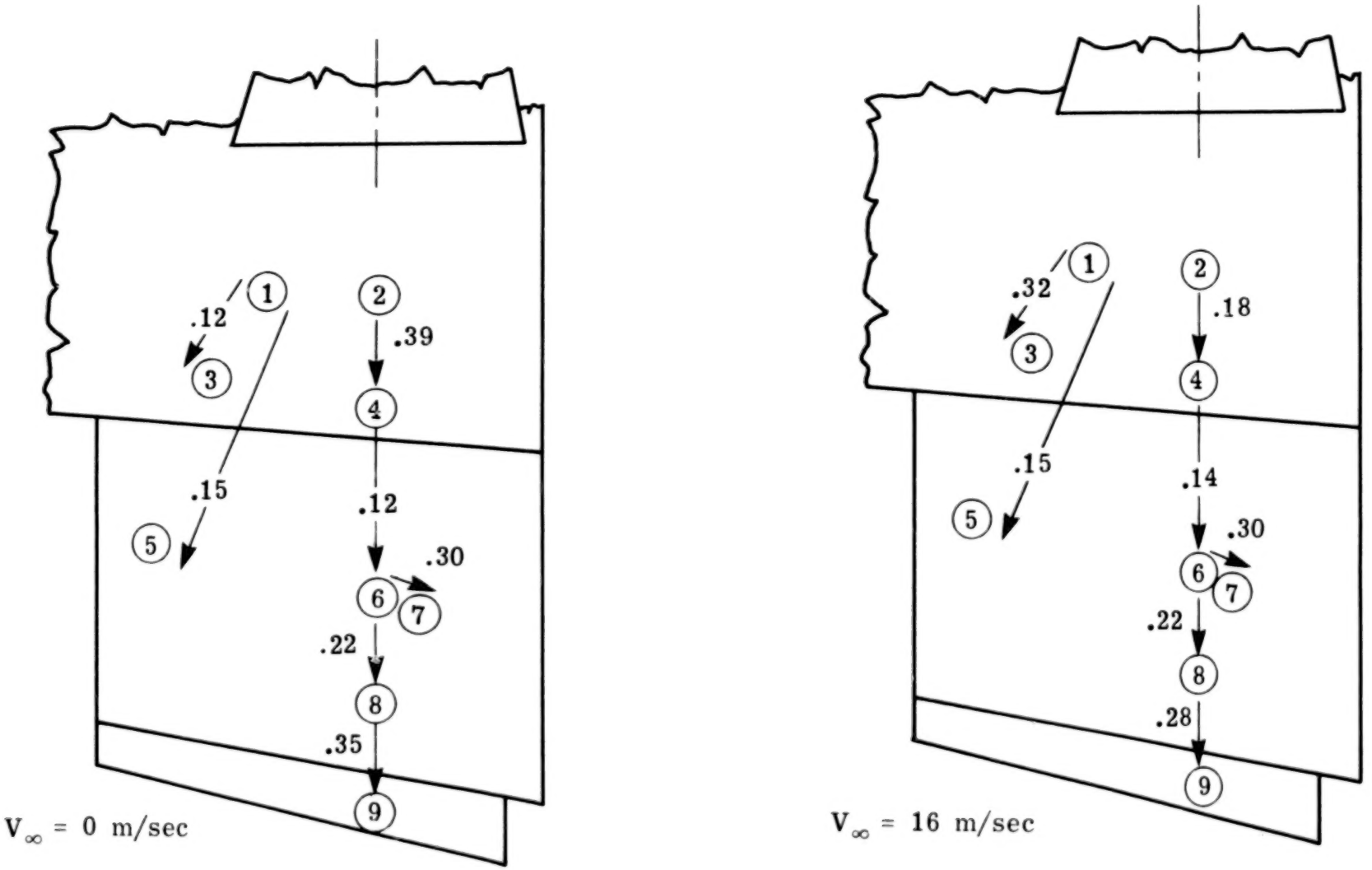

(c) Comparison of cross-correlation coefficients for V_∞ = 0 and 16 m/sec.

Figure 24.- Concluded.

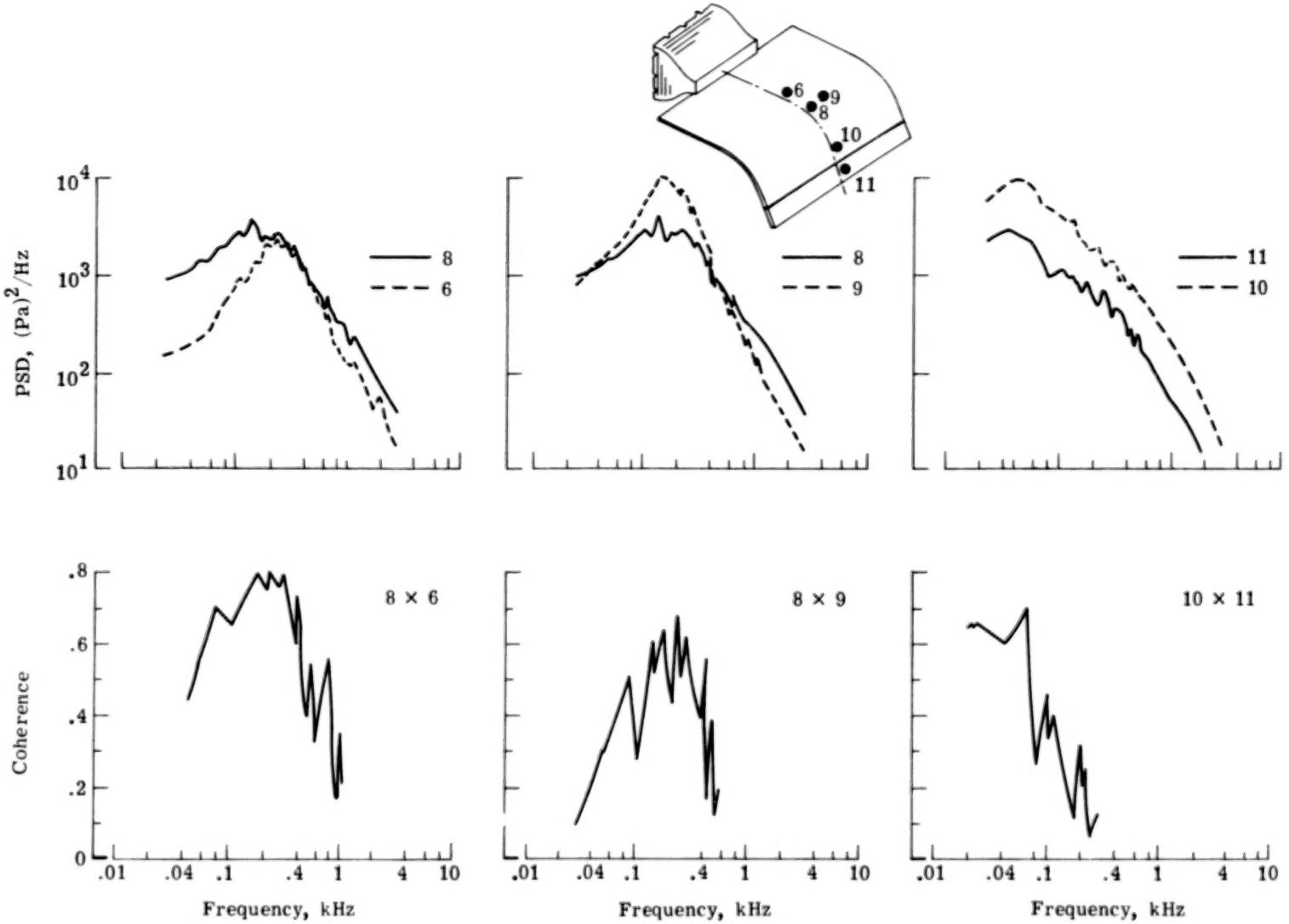

Figure 25.- Coherence function and PSD for three sets of measurement locations for q = 22 kPa.

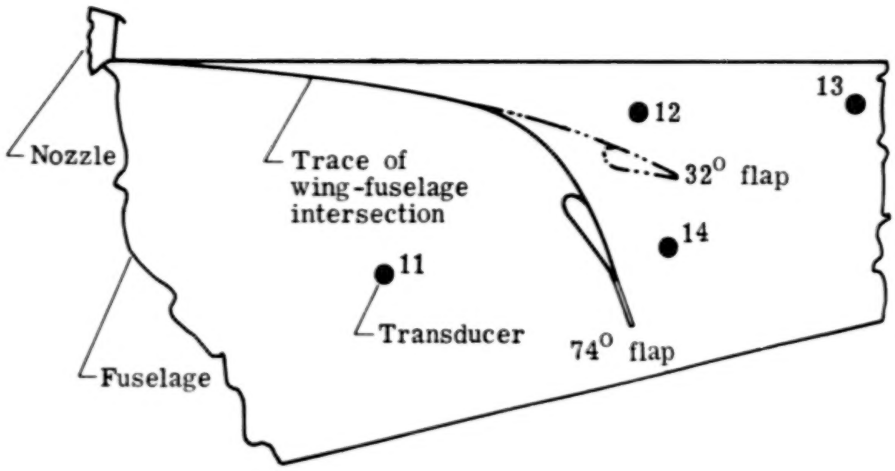

Figure 26.- Location of transducers on fuselage sidewall.

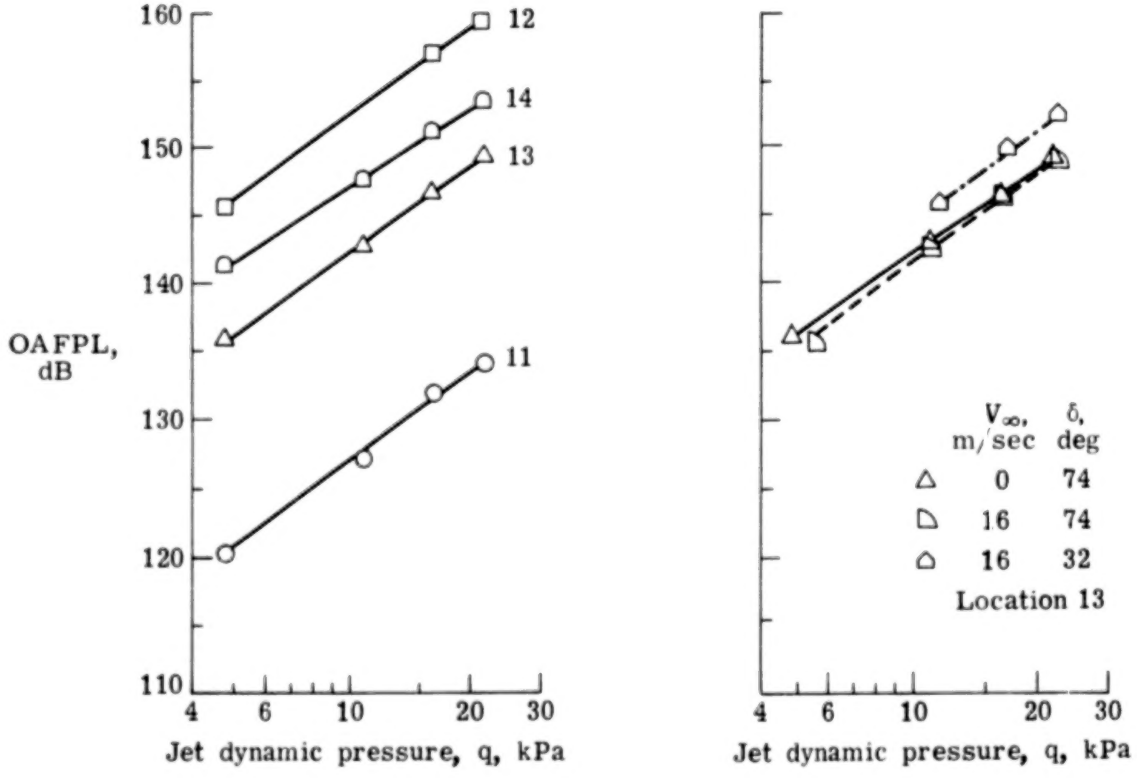

(a) Comparison of loading at four locations for $V_\infty = 0$ and $\delta = 74^\circ$.

(b) Effects of airspeed and flap deflection angle.

Figure 27.- Overall fluctuating pressure level on fuselage sidewall.

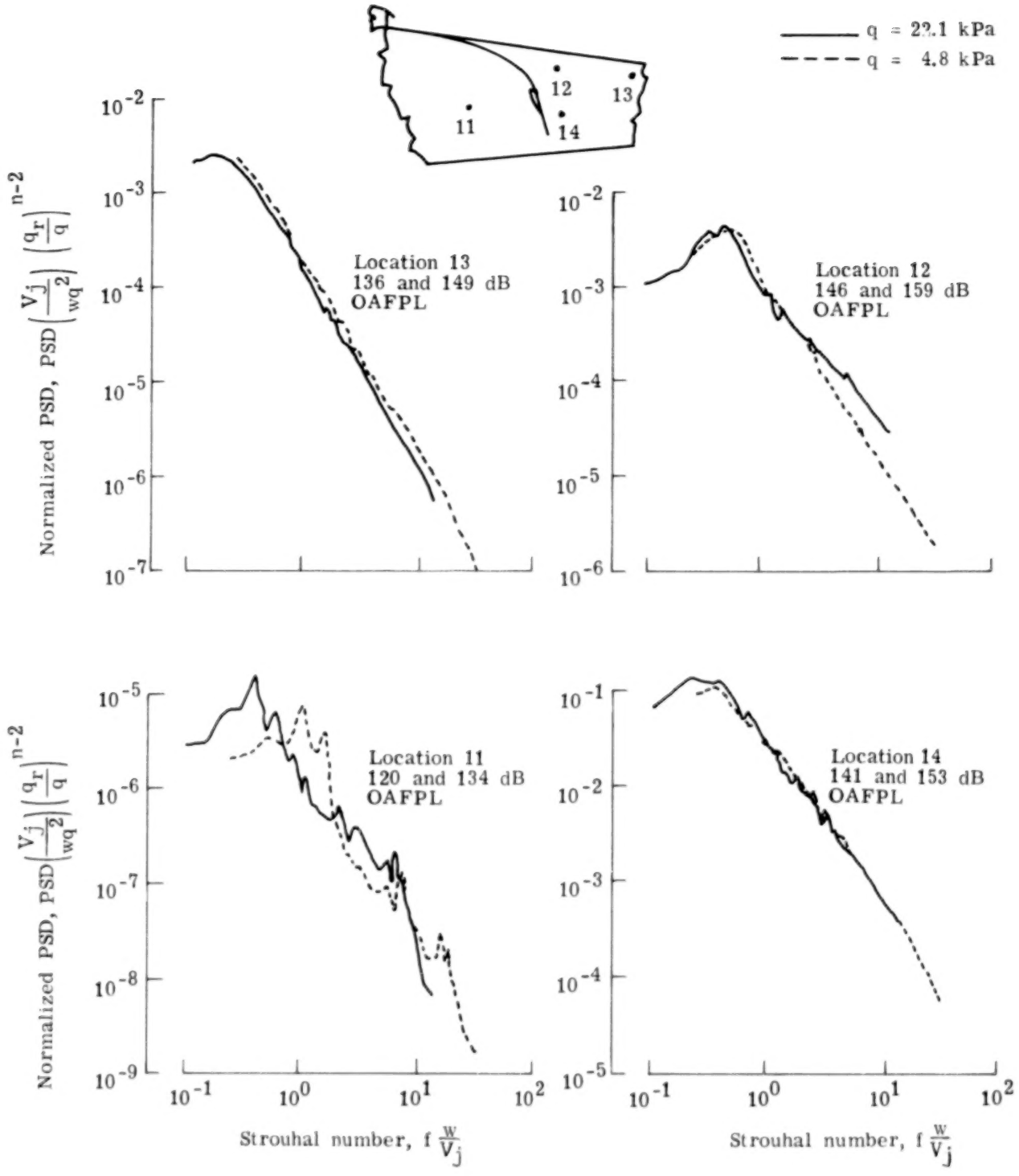

Figure 28.- Normalized spectra for fuselage loads. Configuration 1.2; V_∞ = 0.

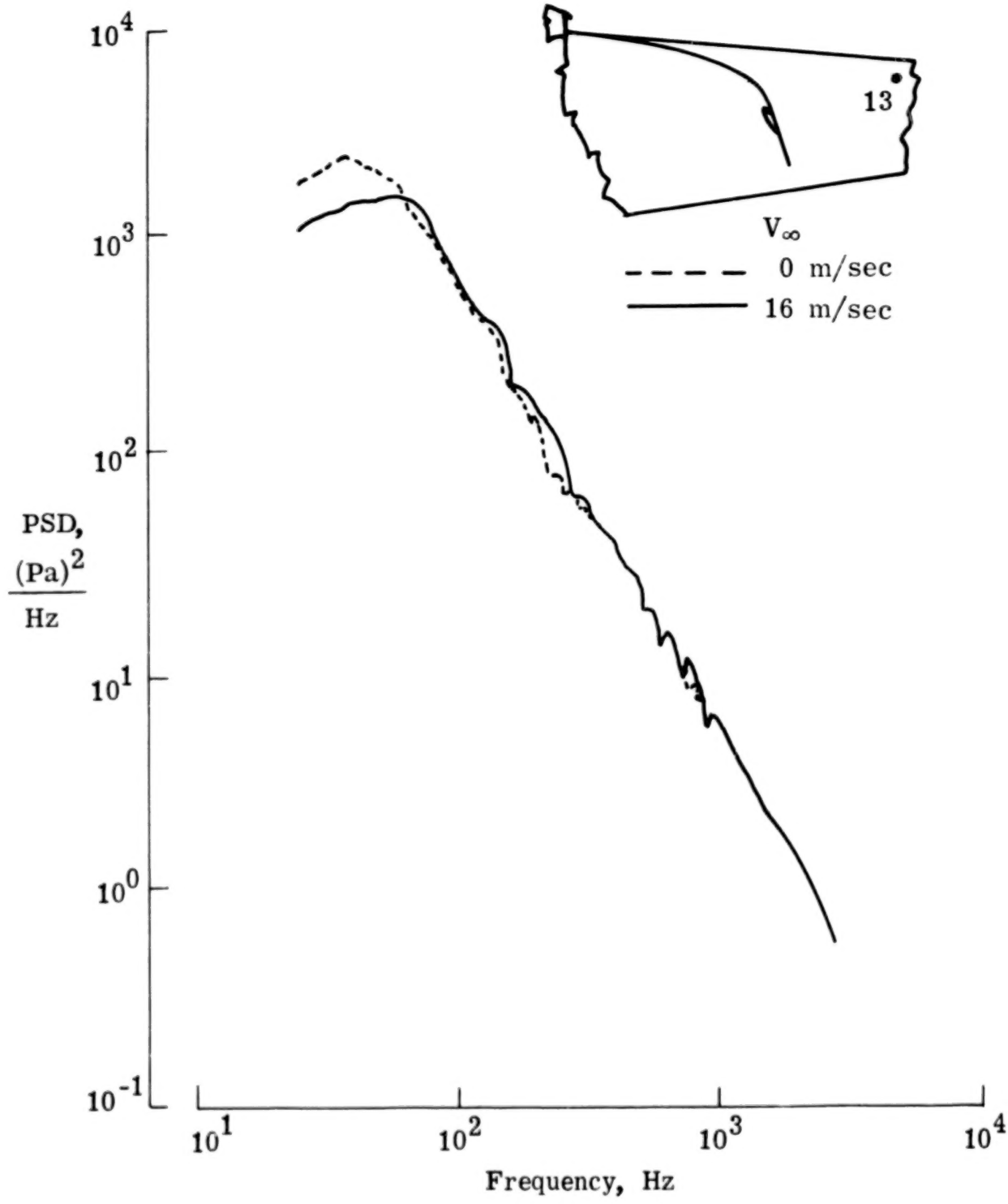

Figure 29.- Effect of airspeed on fuselage fluctuating pressure PSD at location 13 for q = 16.5 kPa.

1. Report No.	2. Government Accession No.	3. Recipient's Catalog No.
NASA TP-1577		

4. Title and Subtitle	5. Report Date
EXPERIMENTAL STUDY OF ACOUSTIC LOADS ON AN UPPER-SURFACE-BLOWN STOL AIRPLANE CONFIGURATION	December 1979
	6. Performing Organization Code

7. Author(s)	8. Performing Organization Report No.
Conrad M. Willis and James A. Schoenster	L-13167
	10. Work Unit No. 505-33-53-03

9. Performing Organization Name and Address	11. Contract or Grant No.
NASA Langley Research Center Hampton, VA 23665	
	13. Type of Report and Period Covered Technical Paper

12. Sponsoring Agency Name and Address	14. Sponsoring Agency Code
National Aeronautics and Space Administration Washington, DC 20546	

15. Supplementary Notes

16. Abstract

Fluctuating pressure levels have been measured on the flap and fuselage of an upper-surface-blown jet-flap airplane configuration in a wind tunnel. The model tested had turbofan engines with a bypass ratio of 3 and a thrust rating of 10 kN. Rectangular nozzles were mounted flush with the upper surface at 35 percent of the wing chord. Test parameters were flap deflection angle, jet impingement angle, angle of attack, free-stream velocity, spanwise location of the engine, and jet dynamic pressure. Load levels were high throughout the jet impingment region, with the highest levels (about 159 dB) occurring on the fuselage and near the knee of the flap. The magnitude of the forward-velocity effect appeared to depend upon the ratio of free-stream and jet velocities. Good agreement was obtained between fluctuating pressure spectra measured at jet dynamic pressures of 7 and 22 kPa when the spectra were scaled by nondimensional functions of dynamic pressure, velocity, and the empirical relationship between dynamic pressure and overall fluctuating pressure level.

17. Key Words (Suggested by Author(s))	18. Distribution Statement
Upper surface blown Acoustic loads Jet impingement	Unclassified - Unlimited Subject Category 71

19. Security Classif. (of this report)	20. Security Classif. (of this page)	21. No. of Pages	22. Price*
Unclassified	Unclassified	54	$5.25

* For sale by the National Technical Information Service, Springfield, Virginia 22161

NASA-Langley, 1979

90 %